Volume 1

Chapter 8

The Anacona Terrane: A Small Early Paleozoic Peri–Gondwanan Terrane in the Cauca–Romeral Fault System

https://doi.org/10.32685/pub.esp.35.2019.08
Published online 21 May 2020

Jorge Julián RESTREPO[1]*, Uwe MARTENS[2], and Wilmer E. GIRALDO–RAMÍREZ[3]

1 jjrestrepoa@gmail.com
Universidad Nacional de Colombia
Sede Medellín
GEMMA Research Group
Medellín, Colombia

2 umartens@s2sgeo.com
S2SGeo
1315 Alma Ave Ste 134, Walnut Creek, CA 94596, USA

3 wegirald@gmail.com
Alcaldía de Marinilla
Calle 30 n.° 30–13
Marinilla, Antioquia, Colombia

* Corresponding author

Abstract The Anacona Terrane is a small terrane south of Medellín that underwent a geologic history dissimilar to that of the adjacent Tahamí Terrane to the east and the Quebradagrande (Ebéjico) Terrane to the west. The metamorphic basement of the Anacona Terrane is relatively old, comprising amphibolites and metasedimentary rocks, with probable late Neoproterozoic depositional ages, and granitic orthogneisses, with Ordovician magmatic ages. The age of the last metamorphic event to affect the Anacona Terrane is constrained to the Devonian or earliest Carboniferous, while Triassic metamorphism, which is widespread in the Tahamí Terrane, has not been documented in the Anacona Terrane, indicating that the terranes were amalgamated during or after the Triassic. Correlatives of the terrane are the Acatlán Complex in southern México and the Marañón Complex and coastal islands in Perú; we surmise that the Anacona Terrane may have originated in a southerly position and migrated northwards, similar to the motion of the Caribbean Plate relative to the South American margin.
Keywords: *Anacona, tectonostratigraphic terranes, Colombian Andes, Proterozoic sedimentation, garnet amphibolites.*

Resumen El Terreno Anacona es un pequeño terreno localizado al sur de Medellín que presenta una historia geológica diferente a la de los terrenos adyacentes, el Tahamí al este y el Quebradagrande (Ebéjico) al oeste. El basamento metamórfico del Terreno Anacona es relativamente antiguo, comprende anfibolitas y rocas metasedimentarias, con probable edad de depositación neoproterozoica tardía, y ortogneises graníticos con edades magmáticas ordovícicas. La edad del último evento metamórfico que afectó al Terreno Anacona está restringida al Devónico o Carbonífero temprano, mientras que el metamorfismo triásico, presente en el Terreno Tahamí, no ha sido registrado en el Terreno Anacona. Lo anterior indica que estos terrenos se amalgamaron durante o después del Triásico. El Complejo Acatlán en el sur de México y el Complejo Marañón y las islas costeras en Perú son equivalentes del Terreno Anacona; proponemos que el Terreno Anacona podría haberse originado en una posición al sur y migrado al norte, siguiendo el desplazamiento de la Placa del Caribe con relación al margen suramericano.
Palabras clave: *Anacona, terrenos tectonoestratigráficos, Andes colombianos, sedimentación proterozoica, anfibolitas granatíferas.*

Citation: Restrepo, J.J., Martens, U. & Giraldo–Ramírez, W.E. 2020. The Anacona Terrane: A small early Paleozoic peri–Gondwanan terrane in the Cauca–Romeral Fault System. In: Gómez, J. & Mateus–Zabala, D. (editors), The Geology of Colombia, Volume 1 Proterozoic – Paleozoic. Servicio Geológico Colombiano, Publicaciones Geológicas Especiales 35, p. 149–165. Bogotá. https://doi.org/10.32685/pub.esp.35.2019.08

1. Introduction

The basement of the Central Cordillera of Colombia comprises low– to high–grade metamorphic rocks of diverse age locally intruded by Triassic, Cretaceous, and Paleogene plutons. Initial studies regarded the metamorphic basement as a single unit, the Ayurá–Montebello Group (Botero, 1963), but it soon became apparent that several metamorphic events had affected this group of rocks. This led to the proposal that the metamorphic basement of the Central Cordillera was a polymetamorphic unit (Restrepo & Toussaint, 1984) and that this metamorphic basement formed the "backbone" of the Tahamí Terrane (Toussaint & Restrepo, 1989; see also Restrepo & Toussaint, 2020).

Mapping conducted in the 1970s and 1980s revealed in detail the nature of the metamorphic basement exposed around the county of Caldas, ca. 20 km south of Medellín (Echeverría, 1973; Sepúlveda & Saldarriaga, 1980; Patiño & Noreña, 1984; Maya & Escobar, 1985). Unlike the majority of the metamorphic basement in the Central Cordillera, which is characterized by low–P assemblages (e.g., Echeverría, 1973), the rocks near Caldas include garnet–bearing amphibolites and kyanite–bearing metapelites indicative of medium–pressure metamorphism (Restrepo & Toussaint, 1977). Furthermore, geochronologic work consistently yielded older ages than the Permian – Triassic metamorphic events detected in the rest of the Tahamí Terrane (Restrepo & Toussaint, 1978; Restrepo et al., 1991). The first Precambrian K–Ar hornblende age of 1650 ± 500 Ma (Restrepo & Toussaint, 1978) was discarded after the same sample was dated again by the same method, yielding ages between 254 ± 9 Ma and 319 ± 48 Ma; in contrast, a K–Ar muscovite age from the granitic orthogneiss yielded an age 343 ± 12 Ma, older than all the other mica ages from gneisses in the Central Cordillera (Restrepo et al., 1991). Recently, more robust U–Pb and ^{40}Ar–^{39}Ar geochronology has confirmed that the metamorphic basement in the Caldas area underwent a different geological evolution compared with the rest of the metamorphic basement of the Tahamí Terrane. It was therefore separated as an independent unit termed the Anacona Terrane (Figure 1; Martens et al., 2014; Restrepo et al., 2009).

Despite its relatively small size, approximately 45 km^2, the Anacona Terrane satisfies the definition of tectonostratigraphic terrane (Coney et al., 1980; Jones et al., 1983); it is a fault–bounded geologic entity or fragment that is characterized by a distinctive geologic history that differs markedly from that of adjacent terranes. Detailed mapping has shown that the Anacona–Tahamí Terrane boundary is a regional north–south trending ductile fault zone, the Santa Isabel Fault (Figure 2; Giraldo–Ramírez, 2013), which is characterized by mylonites and tectonic breccias.

2. Lithology of Units

The two main rock units of the Anacona Terrane are the Caldas Amphibolite and La Miel Orthogneiss (Figure 3a, 3b). The amphibolite is a polyphase metamorphic rock composed mainly of blue–green hornblende + almandine–rich garnet + plagioclase. Unlike the nearby amphibolites of the Tahamí Terrane, the amphibolites in the Anacona Terrane are rich in garnet, up to 30% by volume (Figure 3a). The garnet porphyroblasts are characterized by coronas of hornblende + plagioclase + quartz. Peak amphibolite facies pressure and temperature (PT) conditions were estimated at 1.35 GPa, 630 °C (Bustamante, 2003). These PT conditions are consistent with those established for the mineral assemblages in the metasedimentary schists that are locally interbedded with the amphibolite. These assemblages contain kyanite, garnet, and staurolite, indicating medium–pressure, lower–amphibolite facies conditions. The schists are also polyphase, showing evidence for at least three metamorphic phases (Restrepo, 1986).

Some features are suggestive of the Caldas garnet amphibolite being a retrogressed eclogite: the high garnet content is more typical of eclogite than amphibolite; symplectites of hornblende and plagioclase are common; corona textures of garnet producing amphibole + plagioclase are suggestive of retrogression by decompression (Figure 4). However, despite detailed thin section petrography, it has not been possible to identify relict sodic clinopyroxene (omphacite) in this unit (Martens et al., 2014).

Geochemical analyses of the Caldas Amphibolite (Giraldo–Ramírez, 2013) show a predominance of basaltic protoliths. The rare earth element (REE) patterns (Figure 5) are slightly enriched in light REE, with Ta and Nb anomalies suggesting the presence of subduction–related fluids in the melted source. The REE patterns are transitional between continental arc and E–MORB or continental tholeiite. The trace element geochemistry is inconsistent with the generation of the amphibolite protolith in a typical mid–ocean ridge; instead, it has been proposed that the basaltic protoliths formed in a continental arc (Giraldo–Ramírez, 2013). These features contrast with the geochemical character of Tahamí Terrane amphibolites, which are predominantly MORB tholeiites (Correa–Martínez et al., 2005; Vinasco et al., 2006; Restrepo, 2008; Giraldo, 2010). Sm–Nd isotopic analyses of Caldas Amphibolite are presented in Table 1, showing positive εNd ranging from 2.6 and 5.8 and model ages between 0.89 and 1.19 Ga.

The second major geologic unit in the Anacona Terrane is the granitic, S–type La Miel Orthogneiss, which is composed of quartz + plagioclase + K–feldspar + muscovite + biotite ± garnet. The K–feldspar is mainly orthoclase that has been inverted to microcline. The foliation of the rock is defined by the muscovite and biotite, and locally, a primary mineral tabular

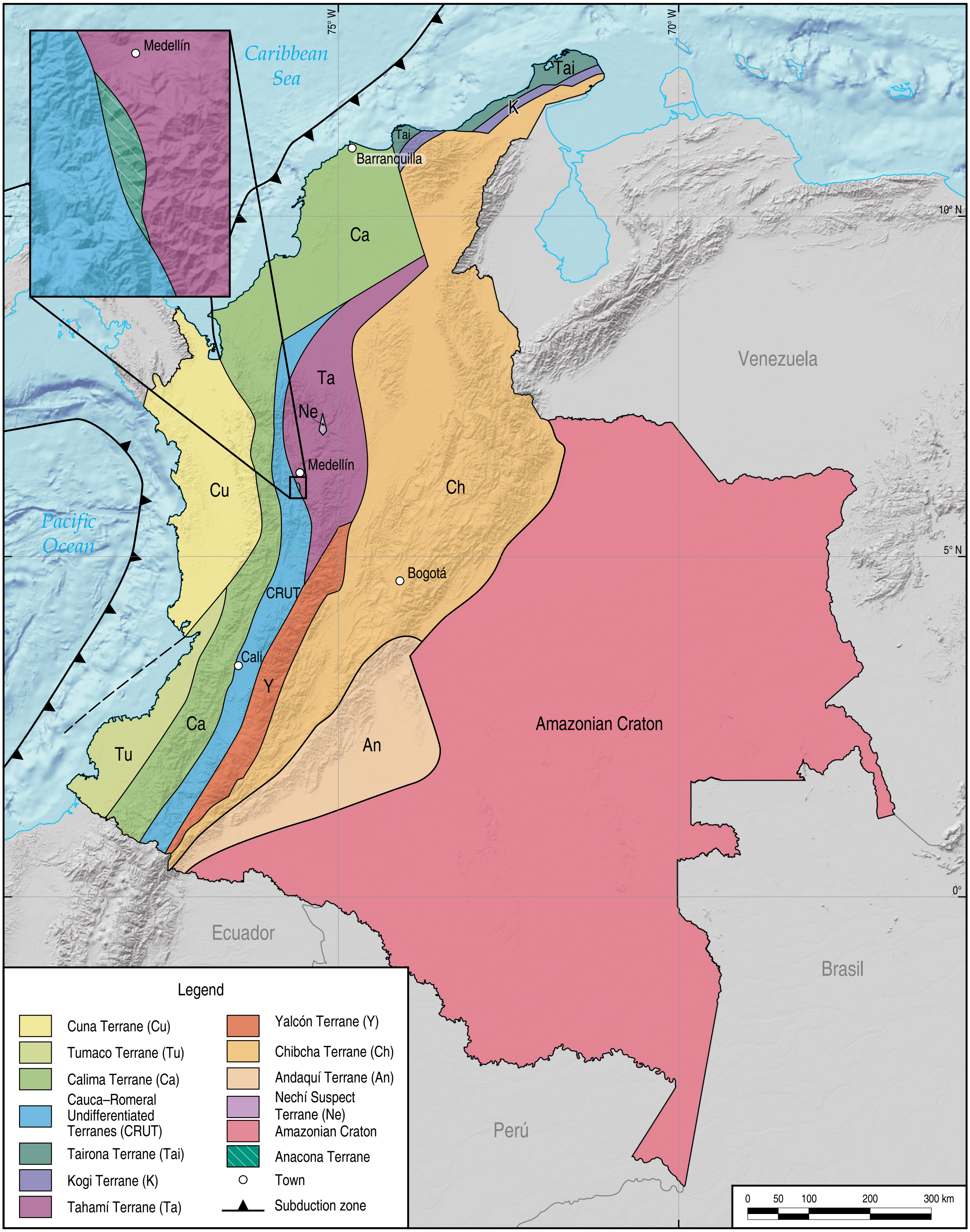

Figure 1. Tectonostratigraphic terranes of Colombia (after Restrepo & Toussaint, 2020).

Carboniferous

Devonian

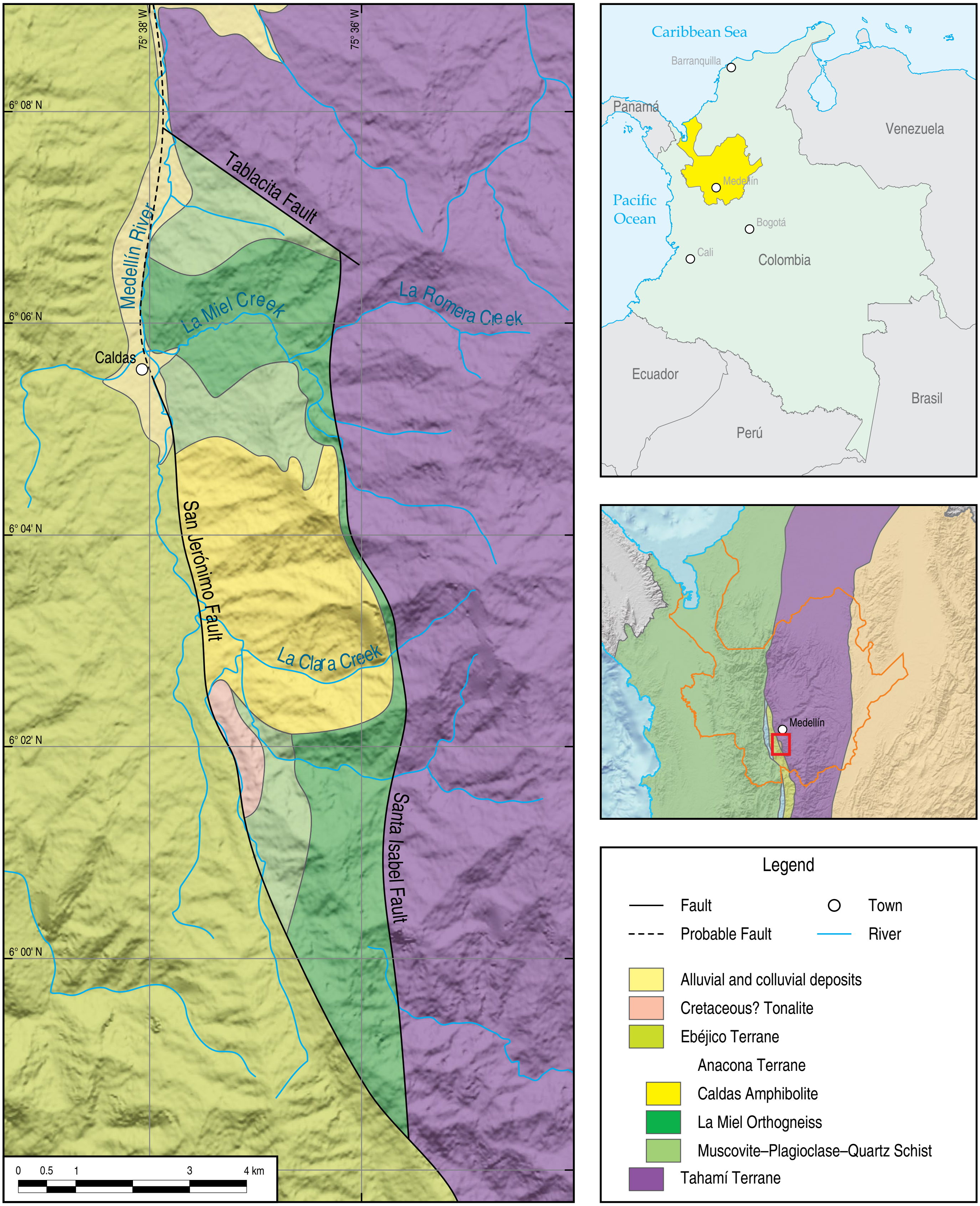

Figure 2. Geologic map of the Anacona Terrane, modified from Giraldo–Ramírez (2013).

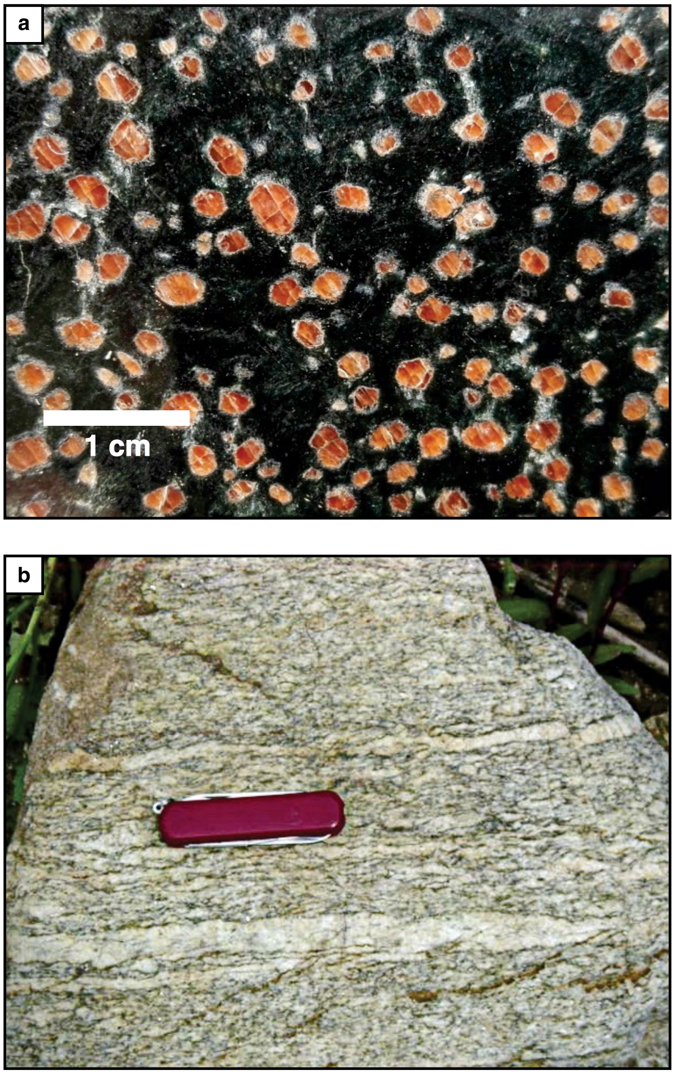

Figure 3. (a) Photographs of a polished slab of the Caldas Amphibolite **(b)** and La Miel Granitic Orthogneiss.

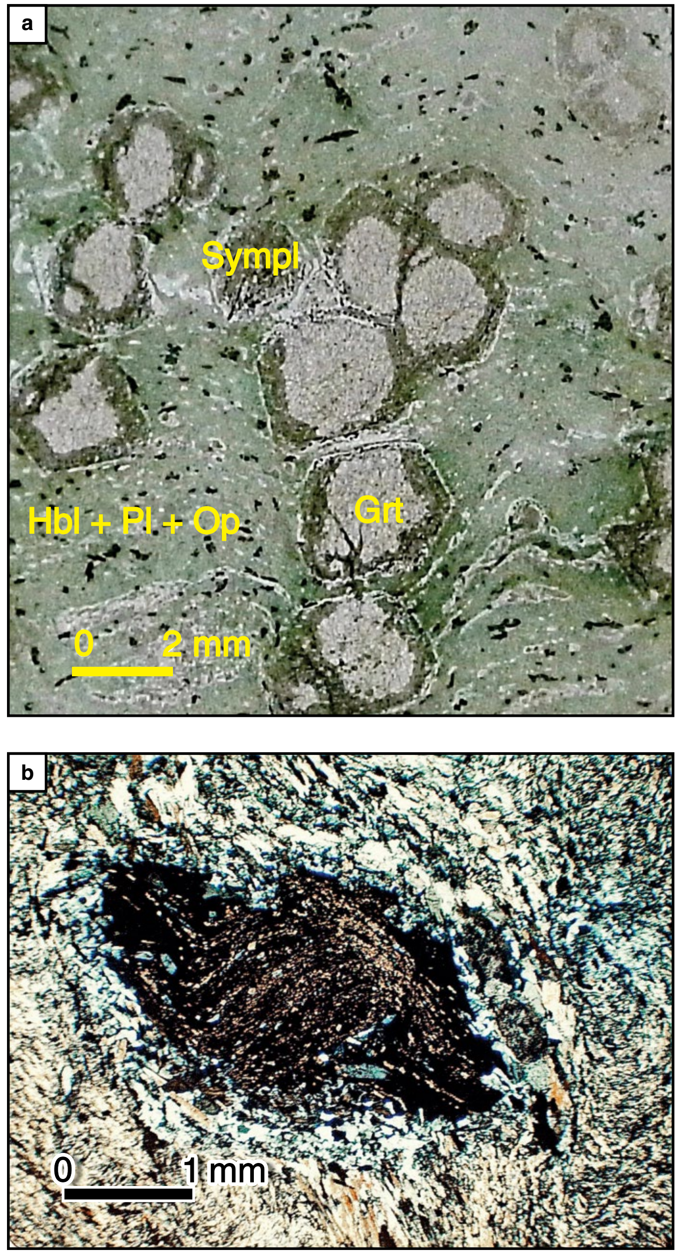

Figure 4. (a) Garnet replaced by a symplectite of plagioclase and hornblende; photomicrograph in plane light (Grt) garnet, (Sympl) symplectite, (Hbl) hornblende, (Pl) plagioclase, (Op) Opaque mineral. **(b)** Garnet with rotational structure and rims replaced by plagioclase and hornblende; photomicrograph in crossed–polarized light (from Restrepo, 1986).

orientation of feldspar is preserved (Figure 3b). Field relations clearly show that La Miel granitic protolith intruded the amphibolites and the associated metamorphic units.

U–Pb zircon geochronology of La Miel Orthogneiss has yielded Ordovician crystallization ages of approximately 445 Ma and 480 Ma in two different samples (Martens et al., 2014), implying an even older protolith age for the Caldas Amphibolite and their associated metasedimentites. ^{40}Ar–^{39}Ar white mica ages of the orthogneiss yielded an age of ca. 345 Ma (Vinasco et al., 2006), which is the best available age constraint for the timing of metamorphism in the Anacona Terrane. This age is consistent with the maximum age of ca. 360 Ma obtained from a U–shaped ^{40}Ar–^{39}Ar hornblende spectrum, which may reflect the incorporation of excess argon (Restrepo et al., 2008). Importantly, none of the ^{40}Ar–^{39}Ar step–heating experiments have revealed any Triassic component, indicating that the Anacona Terrane basement has not experienced the ubiquitous Triassic metamorphism characteristic of the Tahamí Terrane. It therefore seems unlikely that the Anacona Terrane was adjacent to the Tahamí Terrane during high–grade Triassic metamorphism or that it forms the basement to the Tahamí Terrane (Cajamarca Complex), as proposed by Villagómez et al. (2011).

Although less abundant, quartz + muscovite + garnet–bearing quartzites and mica schists are also present in the Anacona Terrane. They occur as metapelitic layers interbedded with the

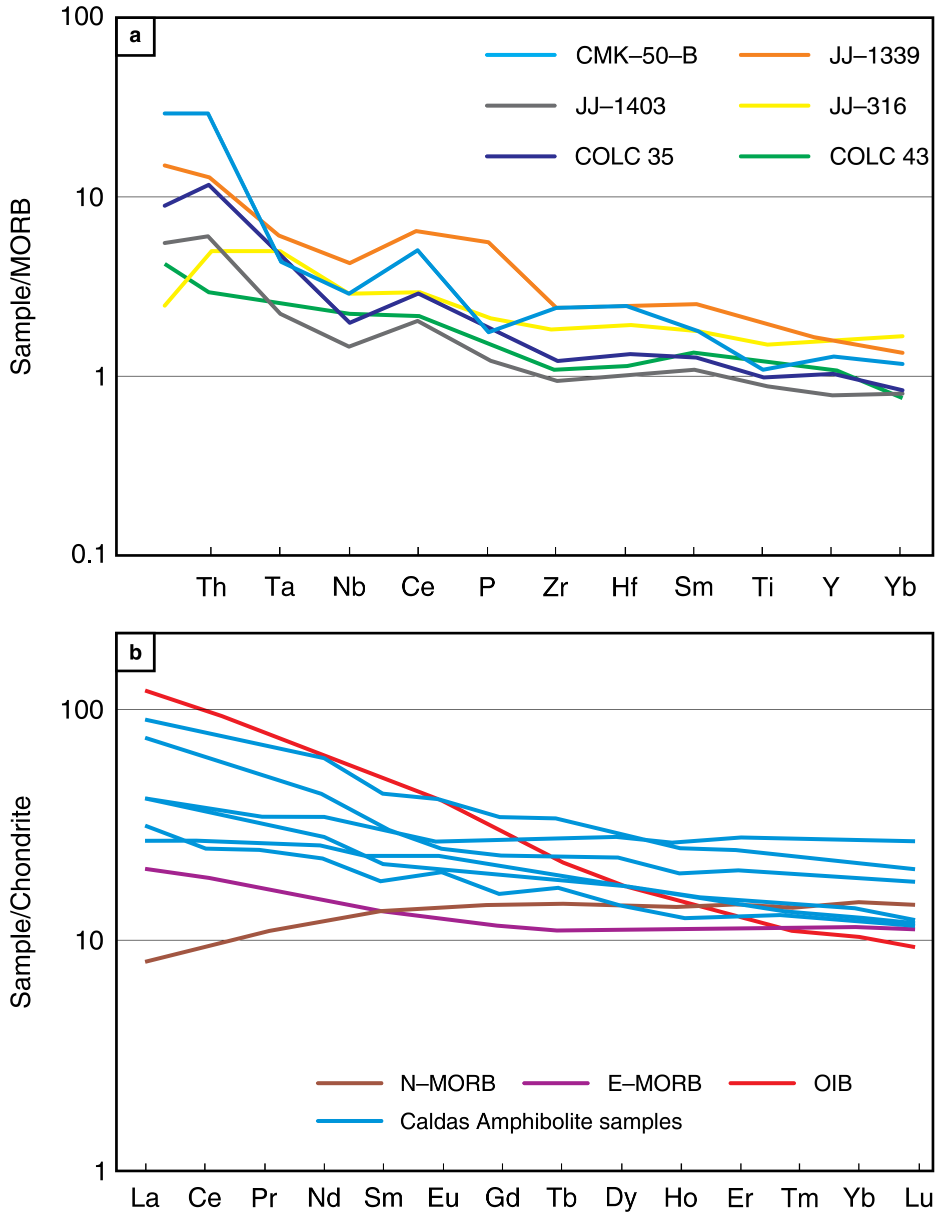

Figure 5. (a) N–MORB (Hofmann, 1988) normalized analyses of the Caldas Amphibolite. Modified from Giraldo–Ramírez (2013). Samples CMK–50–B, JJ–316, JJ–1339 and JJ–1403 from Giraldo–Ramírez (2013) and COLC 35 and COLC 43 from Giraldo (2010). **(b)** Chondrite–normalized Caldas Amphibolite (Boynton, 1984; blue) in comparison with N–MORB, E–MORB and OIB (Sun & McDonough, 1989). Modified from Giraldo–Ramírez (2013).

Table 1. εNd and model ages for three samples of Caldas Amphibolite

Sample	(^{143}Nd/^{144}Nd) 0	(^{147}Sm/^{144}Nd) 0	(^{143}Nd/^{144}Nd)	εNd (700 Ma)	T dm (Ga)
MIG 1	0.513	0.152	0.512	2.612	1.192
MIG 2	0.513	0.172	0.512	5.799	0.891
WG	0.513	0.158	0.512	3.428	1.135

Source: Samples MIG 1 and 2 from Giraldo (2010); sample WG from Giraldo–Ramírez (2013).
Note: Assumed values: (^{143}Nd/^{144}Nd)CHUR = 0.512638, (^{147}Sm/^{144}Nd)CHUR = 0.1967 (De Paolo, 1981).
Present–day composition of the DM: ^{147}Sm/^{144}Nd = 0.222 and ^{143}Nd/^{144}Nd = 0.513114 (Michard et al., 1985).

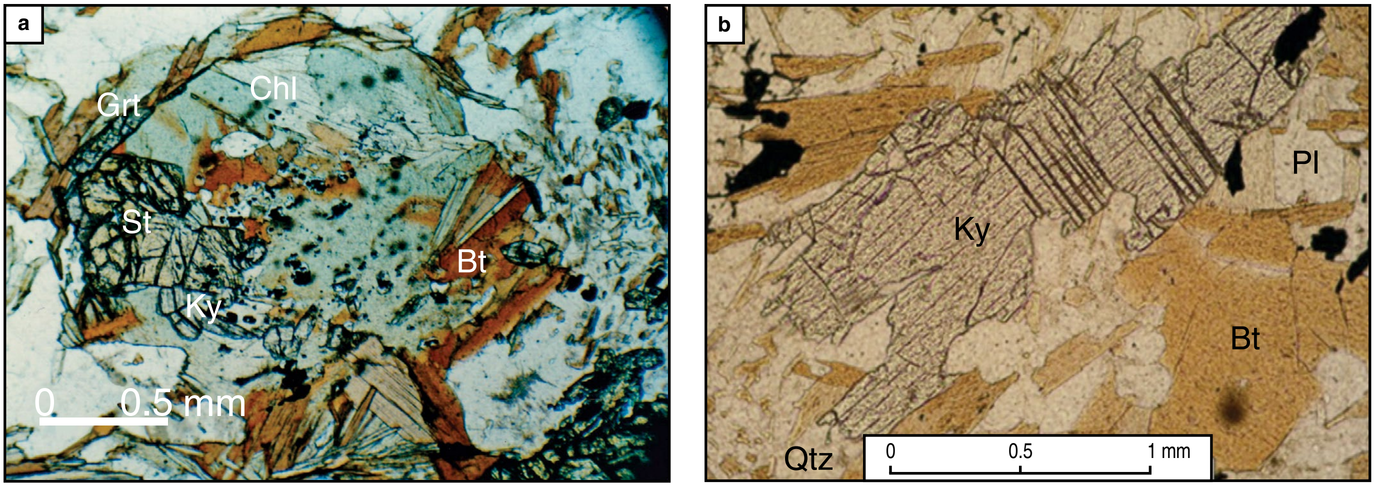

Figure 6. (a) Photomicrograph of pelitic schist interbedded within the Caldas Amphibolite, showing staurolite (St), kyanite (Ky), garnet (Grt), and chloritized (Chl) biotite (Bt). The garnet was partially replaced by biotite. (Mineral abbreviations following Siivola & Schmid, 2007). Taken from Restrepo (1986). **(b)** Kyanite (Ky) crystal with biotite (Bt), quartz (Qtz) and plagioclase (Pl).

amphibolites, and both are intruded by La Miel Orthogneiss. The paragenesis of the pelitic schist includes staurolite, kyanite, garnet, and chloritized biotite (Figure 6). This amphibolite–pelite association likely reflects a volcano–sedimentary sequence metamorphosed under medium pressure, lower–amphibolite facies conditions. The microstructures of the pelitic schist more clearly show the polyphase metamorphic character of the unit (Figure 4b), which underwent at least three tectonic phases (Restrepo, 1986).

Porphyritic dikes of an intermediate composition locally intrude the metamorphic basement of the Anacona Terrane, and range in thickness from 0.5–40 m; a tonalitic pluton also intrudes the metamorphic rocks on the western side. Their ages have yet to be determined. In fact, establishing whether the intrusions are related to magmatism in the Central Cordillera or to magmatic units east of the San Jerónimo Fault would be important in further constraining the geologic evolution of the Anacona Terrane.

3. Terrane Boundaries

To the east, the Santa Isabel Fault separates the Anacona Terrane from the Tahamí Terrane, whereas to the west, the San Jerónimo Fault, the easternmost fault of the Romeral Fault System, separates the Anacona Terrane from the low–grade volcanosedimentary rocks of the Quebradagrande Complex (Figure 2). Both faults run predominantly N–S in the region and define a narrow, near rhombic block at least 20 km long and only 4 km wide at its maximum extent. Mapping by González (1980) suggests that the Anacona Terrane may extend 60 km southwards. The NW–trending Tablacita Fault cuts the Santa Isabel Fault along the northern terrane boundary.

The San Jerónimo Fault, the easternmost strand of the Romeral Fault System, was initially described as an east–dipping reverse fault (Grosse, 1926). At present, most authors regard the San Jerónimo as a dextral strike–slip fault with a reverse component (e.g., Maya & González, 1995). The San Jerónimo Fault exhibits fault–gouge zones up to 3 meters thick (Patiño & Noreña, 1984) along the extent of the Anacona Terrane and a variable trend ranging from N25ºW in the southern segment to N–S in the central and northern segments. The age of movement on the San Jerónimo Fault is constrained by the accretion of the Quebradagrande Complex to the Tahamí Terrane, which is estimated to have occurred at 117–107 Ma (Villagómez et al, 2011), 73–65 Ma (Jaramillo et al., 2017) or 70–58 Ma (Zapata & Cardona, 2017). The timing of accretion of the Anacona Terrane to the Tahamí Terrane is post–Triassic in age, probably occurring in the Late Cretaceous – Paleocene as a consequence of the northward displacement of the Ebéjico and Caribbean Terranes. The Santa Isabel Fault was first mapped by Sepúlveda & Saldarriaga (1980) and Patiño & Noreña (1984). The fault is a strike–slip, mainly ductile structure with a N–S trend and a vertical to 80°W dip. It can be traced from the Versalles–Montebello road in the south (Patiño & Noreña, 1984) to the north, where it ends against the Tablacita Fault. Locally, the fault is characterized by a brittle–ductile tectonic breccia with rock fragments ranging from 1–15 mm in size and embedded in a dark–gray schistose matrix. The breccia fragments include rocks typical of both the Anacona and Tahamí Terranes; some clasts belong to La Miel Orthogneiss, while others are andalusite–bearing schist fragments that are likely derived from the Tahamí Terrane (Giraldo–Ramírez, 2013).

The Tablacita Fault was mapped by Maya & Escobar (1985) and was defined as a terrane boundary by Giraldo–Ramírez (2013). It is a ductile fault trending N55ºW. The fault separates units of the Anacona Terrane to the SW from those of the Tahamí Terrane to the NE. Kinematic indicators show sinistral strike–slip movement and possibly a younger phase of fault movement than that on the Santa Isabel Fault. The Santa Isabel

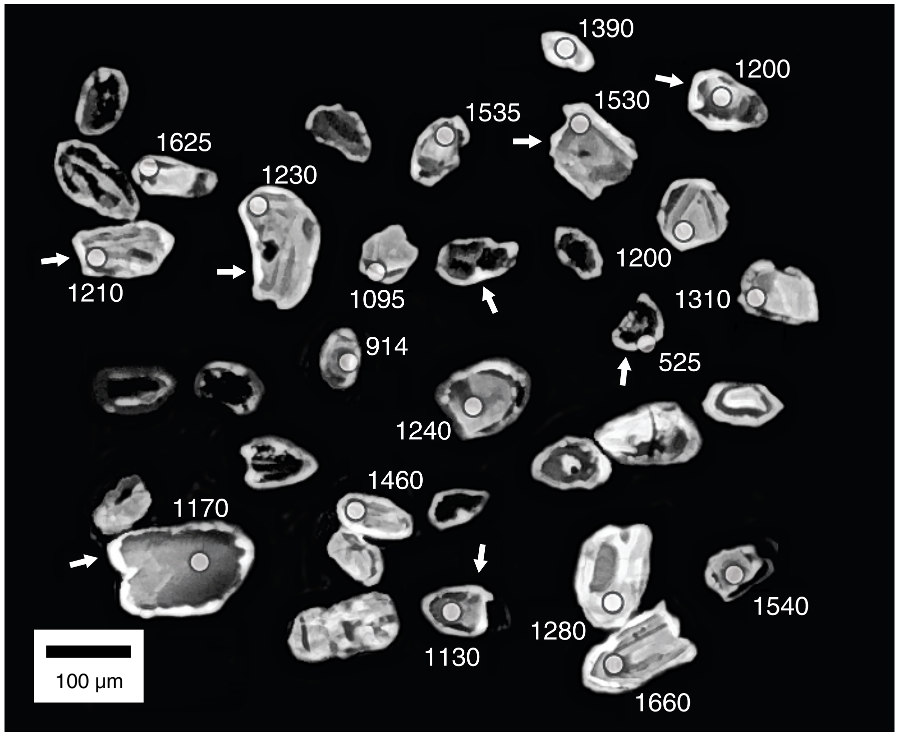

Figure 7. CL imaging of sample AC–1 zircon grains. The numbers are U–Pb ages in Ma. Arrows point to thin metamorphic rims.

and the Tablacita Faults are predominantly ductile in character. They likely formed at a depth greater than 10 km with minor brittle reactivations; there is no evidence for present–day seismic activity (Giraldo–Ramírez, 2013).

4. New Detrital Zircon Geochronology

U–Pb zircon ages were obtained from an Anacona Terrane quartzite collected at the junction between La Romera Creek and La Miel Creek (6° 5' 54'' N, 75° 36' 52'' W). Zircon grains in the sample are anhedral and rounded, and their sizes range from 50–200 µm along their longest dimension (Figure 7). The cathodoluminescence (CL) textures vary from grain to grain and include homogeneous luminescence, concentric zoning, sector zoning, and irregular zones of low luminescence, among others. The roundness and the variety in size and texture attest to the variable nature of the detrital zircon population in the sample. Importantly, CL images reveal thin, luminous, homogenous rims in many of the zircon grains (Figure 7). These rims were likely produced by Paleozoic metamorphism in the Anacona Terrane, but they were too thin to be dated by the method used.

U–Pb geochronology was conducted by LA–ICP–MS at the Laboratorio de Estudios Isotópicos, Centro de Geociencias, UNAM, following the methods described in Solari et al. (2010). Isotopic ratios were corrected for common Pb using the method of Andersen (2002). Ninety–eight grains were dated (Table 2), and they yielded Precambrian ages; hence, $^{207}Pb/^{206}Pb$ ages were preferred. Eight analyses were disregarded because they yielded uncertainties greater than 5%, discordance greater than 4%, or reverse discordance greater than 2%. Hence, 90 analyses were used to construct the probability density diagram in Figure 8.

The detrital zircon signature of the quartzite sample is characterized by a spread in ages from 850 Ma to 1700 Ma. Most of the zircon ages range from 1575–1425 Ma and 1250–1125 Ma. The former population is mostly absent from Laurentian sources (Hoffman, 1989; Martens et al., 2010) but is abundant in Amazonia (Tassinari et al., 2000), a strong indication that the Anacona Terrane is of Gondwanan affinity. The mid–Mesoproterozoic population points to provenance from a Grenville source within Gondwana, such as the Oaxaquia microcontinent (Ortega–Gutiérrez et al., 1995), the Putumayo Orogen (Ibañez–Mejia et al., 2011), or the Arequipa Massif (Wasteneys et al., 1995). A similar feature has been previously observed in the xenocrystic zircon component of La Miel Orthogneiss (Martens et al., 2014, Figure 9).

An important constraint from the geochronology is the time of deposition of the sedimentary protolith of the quartzite. The youngest dated spot yielded an age of 540 ± 75 Ma. However, this age does not necessarily imply a Paleozoic depositional age, because it may correspond to a mixture between a detrital core and a Paleozoic metamorphic rim (see spot in Figure 7). Indeed, the analysis was conducted on an external zone involving part of the detrital core, the metamorphic rim, and epoxy. Furthermore, the Th/U ratio is relatively low, suggestive of a metamorphic isotopic component. It is therefore plausible to in-

Table 2. Corrected zircon U–Pb isotopic ratios, ages, and chondrite–normalized REE concentrations of sample AC–1 (an Anacona Terrane quartzite).

				Corrected ratios[2]									Corrected Ages (Ma)					
	U (ppm)[1]	Th (ppm)[1]	Th/U	$^{207}Pb/^{206}Pb$	±2s abs	$^{207}Pb/^{235}U$	±2s abs	$^{206}Pb/^{238}U$	±2s abs	$^{208}Pb/^{232}Th$	±2s abs	Rho	$^{206}Pb/^{238}U$	±2s	$^{207}Pb/^{235}U$	±2s	$^{207}Pb/^{206}Pb$	±2s
Zircon_001	945	381	0.40	0.0751	0.0018	1.715	0.051	0.1640	0.0025	0.04933	0.00081	0.45	979	14	1014	19	1088	57
Zircon_002	243	154	0.63	0.0782	0.0006	2.149	0.039	0.1980	0.0022	0.05980	0.00180	0.51	1165	12	1167	12	1151	16
Zircon_003	773	240	0.31	0.0859	0.0007	2.800	0.033	0.2325	0.0023	0.06680	0.00200	0.29	1347	12	1355.5	8.9	1336	16
Zircon_004	111	35	0.31	0.0795	0.0041	2.230	0.130	0.2028	0.0031	0.06100	0.00140	0.41	1190	17	1188	41	1180	100
Zircon_005	83	47	0.57	0.0833	0.0057	2.650	0.200	0.2305	0.0042	0.06870	0.00130	0.63	1337	22	1312	57	1260	140
Zircon_006	431	182	0.42	0.0955	0.0012	3.466	0.054	0.2650	0.0031	0.07890	0.00240	0.76	1515	16	1519	12	1537	23
Zircon_007	152	45	0.29	0.0873	0.0019	2.650	0.120	0.2219	0.0066	0.06970	0.00490	0.84	1291	35	1313	33	1364	42
Zircon_008	243	102	0.42	0.0805	0.0009	2.293	0.057	0.2051	0.0022	0.06170	0.00160	0.54	1203	12	1209	18	1208	22
Zircon_009	136	59	0.44	0.0760	0.0013	1.935	0.051	0.1845	0.0031	0.05660	0.00200	0.61	1091	17	1092	18	1099	37
Zircon_010	1766	606	0.34	0.0780	0.0006	2.074	0.028	0.1925	0.0030	0.05950	0.00300	0.66	1135	16	1140.2	9.3	1147	16
Zircon_011	744	295	0.40	0.0776	0.0008	2.082	0.030	0.1941	0.0018	0.05780	0.00074	0.55	1144	10	1142.4	9.9	1136	22
Zircon_012	240	71	0.29	0.0786	0.0005	2.226	0.027	0.2042	0.0021	0.06100	0.00170	0.29	1198	11	1188.9	8.6	1162	12
Zircon_013	451	203	0.45	0.0699	0.0020	1.562	0.040	0.1654	0.0034	0.05030	0.00120	0.45	987	19	955	16	923	58
Zircon_014	825	189	0.23	0.0708	0.0015	1.230	0.029	0.1270	0.0018	0.03854	0.00052	0.13	771	10	814	13	949	44
Zircon_015	719	110	0.15	0.0937	0.0005	3.363	0.028	0.2610	0.0025	0.07610	0.00210	0.56	1495	13	1496.8	6.2	1502	9.2
Zircon_016	225	79	0.35	0.0734	0.0009	1.751	0.036	0.1738	0.0018	0.05170	0.00150	0.46	1033	10	1027	13	1023	24
Zircon_017	291	62	0.21	0.0743	0.0005	1.798	0.040	0.1766	0.0027	0.05390	0.00190	0.80	1048	15	1044	14	1049	12
Zircon_018	334	160	0.48	0.0939	0.0006	3.430	0.036	0.2667	0.0026	0.07840	0.00190	0.61	1524	13	1510.9	8.3	1506	13
Zircon_019	133	97	0.73	0.1005	0.0007	3.982	0.067	0.2884	0.0036	0.08280	0.00250	0.65	1633	18	1630	14	1633	12
Zircon_020	302	100	0.33	0.0814	0.0005	2.292	0.022	0.2063	0.0018	0.06150	0.00150	0.26	1209.3	9.7	1210.8	6.6	1230	12
Zircon_021	386	164	0.43	0.0937	0.0006	3.396	0.035	0.2634	0.0028	0.07830	0.00120	0.61	1507	14	1503.3	8	1501	13
Zircon_022	114	43	0.38	0.0786	0.0009	2.119	0.047	0.1983	0.0027	0.05870	0.00190	0.38	1166	15	1154	15	1162	22
Zircon_023	401	133	0.33	0.0962	0.0006	3.486	0.033	0.2660	0.0026	0.07720	0.00240	0.37	1520	13	1523.8	7.5	1551	11
Zircon_024	195	134	0.69	0.0917	0.0008	3.144	0.057	0.2505	0.0024	0.07330	0.00210	0.70	1441	12	1443	14	1461	17
Zircon_025	505	119	0.23	0.0810	0.0005	2.298	0.025	0.2067	0.0020	0.06440	0.00240	0.68	1211	11	1212.9	7.3	1221	13
Zircon_026	1031	158	0.15	0.0674	0.0018	1.089	0.033	0.1173	0.0039	0.03580	0.00140	0.74	715	23	748	16	849	55
Zircon_027	664	483	0.73	0.0935	0.0040	2.960	0.120	0.2298	0.0043	0.06760	0.00150	0.62	1333	23	1397	30	1495	78
Zircon_028	395	129	0.33	0.0995	0.0006	3.904	0.057	0.2866	0.0042	0.07850	0.00160	0.74	1624	21	1614	12	1615	11
Zircon_029	186	58	0.31	0.0795	0.0006	2.205	0.036	0.2018	0.0020	0.06000	0.00180	0.45	1185	11	1184	11	1185	16
Zircon_030	446	253	0.57	0.0960	0.0012	3.554	0.056	0.2697	0.0030	0.07930	0.00099	0.76	1539	15	1539	12	1546	24
Zircon_031	237	133	0.56	0.0776	0.0022	2.009	0.068	0.1879	0.0026	0.05635	0.00080	0.66	1110	14	1117	23	1155	56
Zircon_032	354	119	0.34	0.0951	0.0009	3.408	0.052	0.2612	0.0029	0.07840	0.00360	0.30	1496	15	1506	12	1529	18
Zircon_033	1240	398	0.32	0.0795	0.0008	2.152	0.038	0.1974	0.0021	0.06020	0.00310	0.87	1161	11	1168	11	1184	20
Zircon_034	271	90	0.33	0.0805	0.0006	2.261	0.040	0.2030	0.0022	0.06130	0.00200	0.35	1191	12	1200	12	1207	16
Zircon_035	408	103	0.25	0.0869	0.0006	2.664	0.049	0.2249	0.0030	0.06770	0.00230	0.77	1308	16	1324	16	1358	13
Zircon_036	76	43	0.56	0.0749	0.0041	1.850	0.110	0.1816	0.0035	0.05530	0.00140	0.63	1076	19	1061	40	1040	120
Zircon_037	516	84	0.16	0.0832	0.0009	2.468	0.043	0.2167	0.0023	0.06453	0.00061	0.71	1264	12	1263	13	1272	21
Zircon_038	748	155	0.21	0.0784	0.0035	1.722	0.086	0.1585	0.0025	0.03830	0.00870	0.66	948	14	1016	32	1149	89
Zircon_039	95	20	0.21	0.0832	0.0021	2.550	0.096	0.2228	0.0045	0.06800	0.00340	0.60	1296	24	1285	28	1271	49

	Chondrite–normalized REE concentrations												
	La	Ce	Pr	Nd	Sm	Eu	Gd	Tb	Dy	Ho	Er	Yb	Lu
Zircon_001	1.11E+01	3.05E+01	1.16E+01	2.12E+01	7.28E+01	1.56E+01	2.24E+02	4.29E+02	7.16E+02	1.24E+03	1.91E+03	3.59E+03	4.64E+03
Zircon_002	1.90E+00	2.46E+01	5.17E+00	1.20E+01	6.31E+01	4.21E+00	2.04E+02	3.63E+02	5.98E+02	9.96E+02	1.45E+03	2.52E+03	3.11E+03
Zircon_003	6.92E-01	2.63E+01	2.30E+00	3.54E+00	1.28E+01	7.99E+00	5.33E+01	1.12E+02	2.04E+02	3.52E+02	5.28E+02	9.66E+02	1.27E+03
Zircon_004	4.98E-01	1.08E+01	9.70E-01	3.48E+00	1.71E+01	5.86E+00	7.49E+01	1.52E+02	2.78E+02	4.91E+02	7.61E+02	1.51E+03	1.90E+03
Zircon_005	1.86E+00	8.56E+00	6.90E+00	1.68E+01	7.30E+01	1.69E+01	2.35E+02	3.78E+02	6.02E+02	9.27E+02	1.27E+03	2.08E+03	2.52E+03
Zircon_006	1.43E+02	1.27E+02	7.87E+01	7.09E+01	8.58E+01	9.06E+00	2.65E+02	4.69E+02	8.20E+02	1.40E+03	2.09E+03	3.74E+03	4.52E+03
Zircon_007	2.32E-01	9.23E+00	9.48E-01	2.30E+00	1.51E+01	4.19E+00	6.98E+01	1.38E+02	2.51E+02	4.60E+02	7.29E+02	1.42E+03	1.85E+03
Zircon_008	1.73E+01	3.30E+01	2.35E+01	4.05E+01	1.22E+02	3.14E+01	4.27E+02	6.95E+02	1.13E+03	1.80E+03	2.45E+03	3.80E+03	4.79E+03
Zircon_009	1.77E-01	8.19E+00	4.25E+00	1.49E+01	7.16E+01	1.12E+01	2.36E+02	3.96E+02	6.51E+02	1.03E+03	1.46E+03	2.45E+03	3.09E+03
Zircon_010	6.96E-01	4.40E+01	3.20E+00	1.22E+01	8.24E+01	4.07E+00	2.79E+02	5.72E+02	9.92E+02	1.70E+03	2.61E+03	4.75E+03	5.69E+03
Zircon_011	5.53E+02	2.90E+02	3.02E+02	2.74E+02	2.77E+02	1.01E+02	3.72E+02	5.60E+02	9.02E+02	1.46E+03	2.26E+03	4.73E+03	6.38E+03
Zircon_012	1.35E-01	2.89E+01	1.64E+00	6.21E+00	3.76E+01	3.37E+00	1.46E+02	2.72E+02	4.88E+02	8.39E+02	1.26E+03	2.31E+03	2.83E+03
Zircon_013	6.96E-01	1.29E+01	1.84E+00	5.47E+00	3.34E+01	1.37E+01	1.66E+02	3.44E+02	6.43E+02	1.19E+03	1.88E+03	3.83E+03	5.03E+03
Zircon_014	1.56E+01	3.12E+01	1.45E+01	1.95E+01	4.21E+01	3.43E+01	7.49E+01	1.43E+02	2.60E+02	4.33E+02	7.55E+02	1.97E+03	3.12E+03
Zircon_015	4.60E-01	5.63E+00	1.62E+00	5.10E+00	3.80E+01	1.94E+00	1.80E+02	4.52E+02	9.51E+02	1.81E+03	3.04E+03	6.30E+03	8.15E+03
Zircon_016	3.46E-01	1.35E+01	4.22E+00	1.29E+01	6.68E+01	1.97E+01	2.56E+02	4.56E+02	7.46E+02	1.25E+03	1.77E+03	2.98E+03	3.81E+03
Zircon_017	1.52E-01	1.57E+01	1.44E+00	4.27E+00	2.40E+01	4.14E+00	8.85E+01	1.79E+02	3.20E+02	5.72E+02	8.93E+02	1.77E+03	2.38E+03
Zircon_018	4.85E-01	1.51E+01	1.89E+00	5.05E+00	2.37E+01	3.61E+00	1.08E+02	2.07E+02	3.70E+02	6.45E+02	9.64E+02	1.66E+03	2.02E+03
Zircon_019	1.81E-01	5.69E+01	1.07E+00	3.87E+00	1.97E+01	9.79E+00	7.31E+01	1.35E+02	2.46E+02	4.32E+02	7.06E+02	1.51E+03	2.05E+03
Zircon_020	7.55E-01	2.07E+01	1.22E+00	4.16E+00	2.38E+01	3.57E+00	1.02E+02	2.01E+02	3.72E+02	6.58E+02	1.01E+03	1.93E+03	2.44E+03
Zircon_021	1.60E-01	1.40E+01	1.68E+00	5.84E+00	3.21E+01	2.97E+00	1.46E+02	2.82E+02	4.99E+02	8.94E+02	1.37E+03	2.44E+03	3.06E+03
Zircon_022	1.14E-01	1.52E+01	1.25E+00	2.98E+00	1.69E+01	7.99E+00	7.61E+01	1.49E+02	2.78E+02	4.96E+02	8.02E+02	1.63E+03	2.13E+03
Zircon_023	3.29E-01	7.13E+00	1.08E+00	4.09E+00	2.33E+01	2.86E+00	1.19E+02	2.57E+02	4.80E+02	8.74E+02	1.35E+03	2.58E+03	3.35E+03
Zircon_024	4.22E-01	1.98E+01	5.18E+00	1.84E+01	8.85E+01	1.71E+01	2.91E+02	4.88E+02	7.63E+02	1.23E+03	1.74E+03	2.82E+03	3.51E+03
Zircon_025	1.35E-01	3.22E+01	8.62E-01	3.74E+00	2.36E+01	2.22E+00	1.19E+02	2.39E+02	4.65E+02	8.32E+02	1.29E+03	2.41E+03	2.86E+03
Zircon_026	2.38E+01	7.88E+01	5.36E+01	5.91E+01	1.53E+02	9.43E+01	2.09E+02	3.48E+02	4.73E+02	6.87E+02	1.07E+03	2.50E+03	3.70E+03
Zircon_027	1.18E+00	8.97E+01	1.12E+01	2.54E+01	7.70E+01	8.21E+01	2.33E+02	3.55E+02	5.61E+02	8.94E+02	1.34E+03	2.66E+03	3.72E+03
Zircon_028	3.97E-01	5.29E+00	4.85E+00	1.95E+01	9.39E+01	1.47E+01	4.02E+02	8.09E+02	1.48E+03	2.36E+03	3.38E+03	5.53E+03	6.59E+03
Zircon_029	1.22E-01	1.05E+01	1.24E+00	3.57E+00	2.20E+01	5.42E+00	1.13E+02	2.20E+02	4.06E+02	6.94E+02	1.06E+03	1.90E+03	2.46E+03
Zircon_030	7.97E-01	2.46E+01	1.44E+00	5.05E+00	2.67E+01	1.08E+01	1.57E+02	3.34E+02	6.70E+02	1.28E+03	2.16E+03	4.58E+03	6.33E+03
Zircon_031	6.96E-01	3.34E+01	3.16E+00	1.11E+01	4.81E+01	1.07E+01	1.85E+02	3.14E+02	5.40E+02	9.14E+02	1.32E+03	2.43E+03	3.20E+03
Zircon_032	1.22E+00	4.32E+01	7.11E+00	1.25E+01	4.21E+01	2.77E+01	1.40E+02	2.28E+02	3.95E+02	6.83E+02	1.04E+03	2.01E+03	2.72E+03
Zircon_033	8.73E-01	4.18E+01	2.41E+00	5.80E+00	2.73E+01	6.96E+00	1.16E+02	2.26E+02	4.54E+02	8.65E+02	1.52E+03	3.47E+03	4.74E+03
Zircon_034	1.14E-01	2.12E+01	1.09E+00	4.20E+00	2.18E+01	2.88E+00	9.20E+01	1.77E+02	3.27E+02	5.81E+02	9.01E+02	1.76E+03	2.31E+03
Zircon_035	1.47E+00	2.18E+01	1.52E+00	5.16E+00	1.85E+01	4.26E+00	6.43E+01	1.47E+02	2.65E+02	4.71E+02	7.32E+02	1.44E+03	1.91E+03
Zircon_036	1.51E+00	7.78E+00	4.53E+00	1.37E+01	6.28E+01	1.99E+01	1.86E+02	3.16E+02	5.20E+02	8.15E+02	1.12E+03	1.91E+03	2.32E+03
Zircon_037	9.11E+00	7.55E+00	4.91E+00	8.75E+00	3.86E+01	5.06E+00	1.95E+02	4.09E+02	6.82E+02	1.05E+03	1.51E+03	2.80E+03	3.39E+03
Zircon_038	3.76E+00	2.14E+01	1.56E+01	2.91E+01	9.39E+01	5.68E+01	1.79E+02	3.16E+02	5.73E+02	8.75E+02	1.34E+03	2.88E+03	3.78E+03
Zircon_039	3.59E-01	7.72E+00	1.19E+00	2.60E+00	1.66E+01	3.61E+00	6.73E+01	1.15E+02	2.17E+02	3.62E+02	5.73E+02	1.06E+03	1.37E+03

Devonian Carboniferous

Table 2. Corrected zircon U–Pb isotopic ratios, ages, and chondrite–normalized REE concentrations of sample AC–1 (an Anacona Terrane quartzite) (*continued*).

				Corrected ratios[2]									Corrected Ages (Ma)						Chondrite–normalized REE concentrations													
	U (ppm)[1]	Th (ppm)[1]	Th/U	$^{207}Pb/^{206}Pb$	±2s abs	$^{207}Pb/^{235}U$	±2s abs	$^{206}Pb/^{238}U$	±2s abs	$^{208}Pb/^{232}Th$	±2s abs	Rho	$^{206}Pb/^{238}U$	±2s	$^{207}Pb/^{235}U$	±2s	$^{207}Pb/^{206}Pb$	±2s	La	Ce	Pr	Nd	Sm	Eu	Gd	Tb	Dy	Ho	Er	Yb	Lu
Zircon_040	314	107	0.34	0.0928	0.0013	3.144	0.075	0.2471	0.0033	0.07250	0.00140	0.80	1423	17	1443	19	1491	30	1.73E-01	1.95E+01	1.14E+00	2.80E+00	1.50E+01	1.01E+01	5.98E+01	1.16E+02	2.26E+02	4.34E+02	7.67E+02	2.13E+03	3.17E+03
Zircon_041	291	56	0.19	0.0719	0.0007	1.605	0.027	0.1616	0.0018	0.04880	0.00140	0.49	966	10	972	11	981	18	1.27E-01	9.72E+00	7.33E-01	3.33E+00	1.77E+01	5.84E+00	6.93E+01	1.29E+02	2.26E+02	3.70E+02	5.39E+02	9.43E+02	1.21E+03
Zircon_042	342	153	0.45	0.0955	0.0007	3.443	0.035	0.2642	0.0029	0.07750	0.00250	0.50	1511	15	1515.8	8.4	1538	14	5.02E-01	1.54E+01	5.55E+00	1.93E+01	1.07E+02	2.08E+01	4.15E+02	7.15E+02	1.22E+03	2.00E+03	2.82E+03	4.42E+03	5.36E+03
Zircon_043	697	51	0.07	0.0929	0.0023	3.260	0.110	0.2547	0.0046	0.07490	0.00130	0.79	1462	24	1472	26	1485	47	1.31E+00	2.46E+00	3.02E+00	4.88E+00	4.59E+01	3.75E+00	2.31E+02	4.28E+02	7.21E+02	9.73E+02	1.28E+03	2.09E+03	2.50E+03
Zircon_044	877	48	0.05	0.0933	0.0007	3.131	0.028	0.2474	0.0035	0.07240	0.00190	0.42	1425	18	1440.3	6.9	1493	14	-8.08E-05	1.96E+00	8.30E-01	3.61E+00	1.89E+01	3.91E+00	8.19E+01	1.44E+02	2.34E+02	4.01E+02	6.98E+02	2.09E+03	3.04E+03
Zircon_045	1018	334	0.33	0.0856	0.0011	2.345	0.036	0.1992	0.0020	0.05895	0.00077	0.58	1171	11	1226	11	1330	24	3.84E+01	7.50E+01	4.20E+01	5.51E+01	1.09E+02	5.63E+00	3.95E+02	6.98E+02	1.16E+03	2.00E+03	2.86E+03	4.57E+03	5.78E+03
Zircon_046	529	62	0.12	0.0937	0.0004	3.436	0.042	0.2657	0.0040	0.07530	0.00320	0.77	1519	20	1512.3	9.6	1501	8.3	1.81E-01	3.23E+00	1.44E+00	6.13E+00	6.75E+01	2.86E+00	3.04E+02	5.24E+02	6.61E+02	7.20E+02	7.53E+02	8.94E+02	9.67E+02
Zircon_047	447	84	0.19	0.0789	0.0028	1.751	0.074	0.1609	0.0032	0.04819	0.00094	0.44	962	18	1027	27	1168	70	6.46E+00	3.08E+02	2.37E+01	3.44E+01	1.36E+02	9.77E+01	5.85E+02	1.14E+03	1.93E+03	3.04E+03	4.48E+03	7.71E+03	9.53E+03
Zircon_048	384	193	0.50	0.0791	0.0004	2.160	0.025	0.1993	0.0022	0.05690	0.00150	0.56	1172	12	1168.1	8.1	1173	11	8.52E-01	2.10E+01	4.91E+00	1.39E+01	6.28E+01	9.79E+00	2.13E+02	3.85E+02	6.26E+02	1.03E+03	1.49E+03	2.56E+03	3.08E+03
Zircon_049	361	102	0.28	0.0801	0.0006	2.306	0.037	0.2083	0.0023	0.06230	0.00190	0.69	1220	12	1214	11	1200	15	7.59E-02	1.92E+01	8.84E-01	2.95E+00	1.61E+01	1.47E+00	6.65E+01	1.30E+02	2.44E+02	4.29E+02	6.96E+02	1.38E+03	1.74E+03
Zircon_050	375	176	0.47	0.0804	0.0006	2.243	0.036	0.2039	0.0023	0.06150	0.00200	0.80	1196	12	1194	11	1209	13	4.10E+00	2.43E+01	4.62E+00	1.15E+01	5.91E+01	1.03E+01	2.67E+02	4.85E+02	8.46E+02	1.40E+03	2.05E+03	3.55E+03	4.33E+03
Zircon_051	367	223	0.61	0.1001	0.0010	3.857	0.077	0.2798	0.0029	0.08210	0.00220	0.39	1591	15	1604	16	1625	19	3.25E-01	4.32E+01	3.13E+00	1.15E+01	5.20E+01	2.79E+01	1.58E+02	2.97E+02	4.94E+02	8.52E+02	1.29E+03	2.48E+03	3.31E+03
Zircon_052	153	47	0.31	0.0794	0.0015	2.260	0.068	0.2052	0.0025	0.06310	0.00280	0.88	1203	13	1198	21	1189	36	1.43E-01	8.91E+00	9.59E-01	3.39E+00	1.95E+01	4.09E+00	8.94E+01	1.69E+02	2.97E+02	5.18E+02	7.93E+02	1.50E+03	1.91E+03
Zircon_053	317	107	0.34	0.0806	0.0005	2.363	0.032	0.2112	0.0021	0.06250	0.00200	0.26	1235	11	1231.2	9.5	1212	12	1.18E-01	2.77E+01	1.41E+00	4.79E+00	2.55E+01	2.63E+00	1.23E+02	2.39E+02	4.22E+02	7.45E+02	1.13E+03	2.15E+03	2.77E+03
Zircon_054	241	93	0.39	0.0813	0.0009	2.300	0.047	0.2063	0.0021	0.06210	0.00150	0.39	1209	11	1215	13	1229	22	4.89E+00	2.12E+01	4.09E+00	5.71E+00	1.97E+01	3.32E+00	8.04E+01	1.50E+02	2.80E+02	5.02E+02	7.86E+02	1.60E+03	2.08E+03
Zircon_055	429	78	0.18	0.0760	0.0006	1.887	0.022	0.1812	0.0019	0.05490	0.00160	0.39	1073	10	1076.3	7.9	1095	15	2.15E-01	1.72E+01	1.48E+00	3.79E+00	2.05E+01	4.51E+00	9.50E+01	1.87E+02	3.54E+02	6.17E+02	9.58E+02	1.76E+03	2.24E+03
Zircon_056	292	51	0.17	0.0954	0.0007	3.548	0.057	0.2708	0.0036	0.08270	0.00270	0.78	1545	18	1537	13	1536	15	2.36E-01	7.81E+00	1.57E+00	4.27E+00	2.78E+01	5.35E+00	1.18E+02	2.30E+02	4.04E+02	7.16E+02	1.07E+03	1.95E+03	2.52E+03
Zircon_057	559	189	0.34	0.0803	0.0006	2.210	0.042	0.2033	0.0025	0.06140	0.00210	0.25	1193	13	1184	13	1205	16	-7.59E-05	3.61E+01	2.03E+00	5.03E+00	3.82E+01	4.26E+00	1.71E+02	3.45E+02	6.26E+02	1.10E+03	1.70E+03	3.07E+03	3.63E+03
Zircon_059	990	419	0.42	0.0884	0.0010	2.706	0.046	0.2220	0.0034	0.06570	0.00150	0.96	1292	18	1330	13	1391	20	8.10E+00	5.22E+01	3.01E+01	5.58E+01	1.74E+02	1.44E+02	4.02E+02	6.79E+02	1.13E+03	1.82E+03	2.61E+03	4.88E+03	6.79E+03
Zircon_060	305	106	0.35	0.0951	0.0008	3.606	0.047	0.2728	0.0029	0.08100	0.00230	0.39	1555	15	1551	10	1533	15	4.22E-01	7.10E+00	2.66E+00	9.45E+00	5.28E+01	1.08E+01	1.97E+02	3.45E+02	5.72E+02	9.38E+02	1.38E+03	2.48E+03	3.21E+03
Zircon_061	1665	74	0.04	0.0910	0.0007	2.979	0.031	0.2389	0.0032	0.06920	0.00180	0.84	1381	17	1402.3	8	1445	14	9.11E+00	9.74E+00	1.02E+01	1.41E+01	4.35E+01	2.82E+01	1.37E+02	3.47E+02	7.22E+02	1.30E+03	2.22E+03	5.02E+03	6.90E+03
Zircon_062	163	58	0.35	0.0802	0.0012	2.349	0.053	0.2108	0.0031	0.06470	0.00210	0.29	1233	16	1227	16	1202	31	5.91E-02	1.53E+01	8.30E-01	2.78E+00	1.50E+01	2.68E+00	5.93E+01	1.13E+02	2.11E+02	3.66E+02	5.88E+02	1.14E+03	1.54E+03
Zircon_063	790	52	0.07	0.0584	0.0020	0.697	0.038	0.0846	0.0035	0.02620	0.00110	0.75	524	21	537	23	541	74	1.98E+02	1.68E+02	1.26E+02	1.16E+02	1.12E+02	6.71E+01	1.34E+02	2.22E+02	2.93E+02	4.36E+02	6.19E+02	1.43E+03	2.41E+03
Zircon_064	315	98	0.31	0.0968	0.0013	3.660	0.054	0.2748	0.0035	0.08120	0.00220	0.42	1565	18	1563	12	1563	26	2.36E+01	5.22E+01	4.31E+01	5.03E+01	8.31E+01	3.46E+01	2.15E+02	3.38E+02	5.34E+02	8.70E+02	1.25E+03	2.35E+03	3.12E+03
Zircon_065	311	78	0.25	0.0847	0.0014	2.683	0.055	0.2295	0.0032	0.06830	0.00270	0.09	1332	17	1323	15	1309	32	1.35E-01	1.86E+01	2.06E+00	9.39E+00	3.56E+01	3.91E+00	1.78E+02	3.04E+02	5.29E+02	8.90E+02	1.27E+03	2.17E+03	2.86E+03
Zircon_066	285	83	0.29	0.0800	0.0005	2.330	0.032	0.2104	0.0024	0.06330	0.00220	0.27	1231	13	1221.4	9.7	1197	12	1.43E+01	3.25E+01	2.11E+01	3.26E+01	7.30E+01	1.99E+01	2.13E+02	3.60E+02	6.30E+02	1.04E+03	1.57E+03	2.71E+03	3.37E+03
Zircon_067	714	197	0.28	0.0690	0.0014	1.369	0.035	0.1442	0.0022	0.04381	0.00050	0.66	869	12	876	15	896	43	7.22E+00	3.13E+01	2.45E+01	4.73E+01	1.80E+02	1.05E+02	4.19E+02	7.29E+02	1.15E+03	1.72E+03	2.40E+03	4.11E+03	5.08E+03
Zircon_068	105	73	0.70	0.0690	0.0012	1.487	0.040	0.1564	0.0022	0.04710	0.00140	0.37	937	12	924	16	896	35	5.15E-01	2.76E+01	7.06E+00	2.24E+01	8.68E+01	5.15E+01	2.56E+02	3.77E+02	5.62E+02	8.15E+02	1.08E+03	1.66E+03	2.04E+03
Zircon_069	1930	1056	0.55	0.0790	0.0003	2.164	0.026	0.1984	0.0021	0.06220	0.00170	0.77	1167	11	1169.2	8.2	1171.6	7.6	1.05E+02	1.66E+02	6.90E+01	6.56E+01	1.51E+02	1.85E+01	5.78E+02	1.09E+03	1.95E+03	3.32E+03	4.95E+03	8.11E+03	9.63E+03
Zircon_070	963	92	0.10	0.0835	0.0007	2.562	0.039	0.2216	0.0027	0.06790	0.00250	0.81	1290	14	1289	11	1281	16	2.56E+00	2.23E+01	1.15E+01	2.23E+01	8.11E+01	5.52E+01	1.87E+02	2.96E+02	4.11E+02	5.07E+02	6.13E+02	8.45E+02	9.35E+02
Zircon_071	390	12	0.03	0.0701	0.0004	1.574	0.028	0.1611	0.0016	0.05140	0.00290	0.80	962.9	8.8	960	11	931	12	1.52E-01	2.79E+00	4.09E-01	1.20E+00	4.46E+00	6.75E+00	1.98E+01	3.17E+01	4.65E+01	6.28E+01	8.09E+01	1.18E+02	1.43E+02
Zircon_072	855	215	0.25	0.0766	0.0004	1.996	0.024	0.1881	0.0017	0.05660	0.00160	0.63	1111.2	9	1114	8.1	1111	11	4.39E-01	1.44E+01	1.61E+00	2.19E+00	8.31E+00	1.12E+01	3.39E+01	8.28E+01	1.89E+02	4.18E+02	8.05E+02	2.27E+03	3.28E+03
Zircon_073	1503	121	0.08	0.0933	0.0006	3.131	0.038	0.2458	0.0036	0.07480	0.00530	0.85	1417	18	1444	11	1493	13	8.82E+00	1.56E+01	1.50E+01	2.39E+01	7.77E+01	4.80E+01	2.65E+02	6.10E+02	1.23E+03	2.09E+03	3.19E+03	6.16E+03	7.67E+03
Zircon_074	567	191	0.34	0.0784	0.0010	2.204	0.041	0.2041	0.0021	0.06050	0.00180	0.17	1198	11	1182	13	1156	25	1.48E-01	3.18E+01	9.38E-01	3.35E+00	2.77E+01	1.33E+00	1.32E+02	2.70E+02	4.72E+02	8.33E+02	1.29E+03	2.47E+03	3.11E+03
Zircon_075	1437	200	0.14	0.0688	0.0003	1.457	0.020	0.1521	0.0019	0.03930	0.00110	0.62	912	10	912.5	8.2	893.9	8.6	2.53E-01	5.02E+00	1.10E+00	6.08E+00	3.92E+01	8.88E+00	1.63E+02	2.78E+02	3.82E+02	4.76E+02	5.51E+02	6.99E+02	7.92E+02
Zircon_076	362	130	0.36	0.0788	0.0006	2.111	0.030	0.1956	0.0019	0.05780	0.00110	0.54	1152	10	1151.9	9.7	1165	14	3.04E-01	2.42E+01	1.64E+00	4.22E+00	2.30E+01	3.23E+00	1.05E+02	2.04E+02	3.73E+02	6.55E+02	1.04E+03	2.02E+03	2.56E+03
Zircon_077	962	252	0.26	0.0733	0.0012	1.663	0.020	0.1652	0.0020	0.04970	0.00085	0.16	986	11	994.4	7.7	1021	32	9.54E-01	2.89E+01	4.63E+00	1.14E+01	6.42E+01	1.35E+01	2.77E+02	5.01E+02	8.62E+02	1.54E+03	2.36E+03	4.32E+03	5.49E+03
Zircon_079	405	134	0.33	0.0788	0.0008	2.267	0.048	0.2067	0.0026	0.06090	0.00190	0.28	1211	14	1202	15	1167	19	1.39E-01	2.88E+01	1.06E+00	4.20E+00	2.76E+01	2.01E+00	1.28E+02	2.62E+02	4.67E+02	8.14E+02	1.24E+03	2.42E+03	3.01E+03
Zircon_080	605	138	0.23	0.0779	0.0003	2.103	0.015	0.1953	0.0018	0.05850	0.00170	0.66	1150	9.7	1149.8	5	1146.1	9.1	9.28E-02	2.71E+01	8.41E-01	2.54E+00	1.16E+01	4.44E+00	5.83E+01	1.26E+02	2.59E+02	4.82E+02	8.25E+02	1.92E+03	2.63E+03

Table 2. Corrected zircon U–Pb isotopic ratios, ages, and chondrite–normalized REE concentrations of sample AC–1 (an Anacona Terrane quartzite) (*continued*).

				Corrected ratios[2]									Corrected Ages (Ma)						Chondrite–normalized REE concentrations													
	U (ppm)[1]	Th (ppm)[1]	Th/U	$^{207}Pb/^{206}Pb$	±2s abs	$^{207}Pb/^{235}U$	±2s abs	$^{206}Pb/^{238}U$	±2s abs	$^{208}Pb/^{232}Th$	±2s abs	Rho	$^{206}Pb/^{238}U$	±2s	$^{207}Pb/^{235}U$	±2s	$^{207}Pb/^{206}Pb$	±2s	La	Ce	Pr	Nd	Sm	Eu	Gd	Tb	Dy	Ho	Er	Yb	Lu
Zircon_081	300	77	0.26	0.0774	0.0009	2.213	0.043	0.2047	0.0027	0.05530	0.00160	0.18	1201	14	1185	14	1132	22	5.49E-01	1.45E+01	1.13E+00	3.17E+00	1.07E+01	1.79E+00	5.06E+01	1.05E+02	2.14E+02	3.97E+02	6.28E+02	1.30E+03	1.70E+03
Zircon_082	172	63	0.36	0.0917	0.0008	3.205	0.057	0.2521	0.0042	0.07480	0.00230	0.70	1449	22	1461	15	1461	16	1.39E+01	3.03E+01	2.16E+01	2.69E+01	3.31E+01	7.82E+00	1.09E+02	1.95E+02	3.60E+02	6.20E+02	9.29E+02	1.74E+03	2.24E+03
Zircon_083	349	77	0.22	0.0696	0.0012	1.472	0.030	0.1529	0.0017	0.04642	0.00059	0.37	917.4	9.5	919	12	914	35	7.17E-02	7.83E+00	4.74E-01	8.75E-01	3.18E+00	6.20E+00	1.67E+01	3.57E+01	6.79E+01	1.33E+02	2.26E+02	5.78E+02	9.31E+02
Zircon_084	213	74	0.35	0.0819	0.0030	2.197	0.066	0.1986	0.0038	0.05928	0.00086	0.28	1168	21	1180	21	1238	70	2.24E-01	1.90E+01	1.65E+00	4.81E+00	2.85E+01	8.35E+00	1.08E+02	2.14E+02	3.94E+02	7.01E+02	1.10E+03	2.17E+03	2.80E+03
Zircon_085	265	86	0.32	0.0817	0.0014	2.348	0.063	0.2082	0.0024	0.06220	0.00250	0.43	1219	13	1226	19	1237	33	1.10E-01	1.58E+01	1.13E+00	3.33E+00	1.91E+01	2.42E+00	8.99E+01	1.87E+02	3.24E+02	5.51E+02	8.53E+02	1.64E+03	2.11E+03
Zircon_086	251	43	0.17	0.0888	0.0007	3.005	0.060	0.2448	0.0029	0.08060	0.00390	0.06	1412	15	1408	15	1399	16	3.80E-02	1.76E+01	9.27E-01	3.54E+00	2.45E+01	1.49E+01	9.35E+01	1.82E+02	3.26E+02	5.71E+02	9.04E+02	1.86E+03	2.68E+03
Zircon_087	141	36	0.26	0.0835	0.0012	2.640	0.063	0.2285	0.0031	0.06680	0.00230	0.23	1326	16	1311	17	1279	29	3.29E+00	1.47E+01	3.23E+00	4.16E+00	1.01E+01	1.08E+00	3.77E+01	7.98E+01	1.61E+02	3.16E+02	5.39E+02	1.19E+03	1.67E+03
Zircon_088	307	177	0.58	0.1020	0.0017	3.412	0.069	0.2442	0.0040	0.07120	0.00160	0.71	1408	21	1507	16	1659	30	1.73E+00	3.37E+01	4.59E+00	9.02E+00	2.77E+01	1.71E+01	8.59E+01	1.45E+02	2.78E+02	5.11E+02	8.99E+02	2.25E+03	3.43E+03
Zircon_089	114	59	0.51	0.0905	0.0012	3.161	0.061	0.2510	0.0031	0.07340	0.00210	0.41	1443	16	1447	15	1435	24	2.57E-01	1.08E+01	1.06E+00	4.70E+00	2.78E+01	5.63E+00	1.21E+02	2.26E+02	4.00E+02	7.07E+02	1.06E+03	1.92E+03	2.56E+03
Zircon_090	170	66	0.39	0.0964	0.0007	3.613	0.041	0.2724	0.0027	0.08130	0.00250	0.38	1553	14	1552.1	9.1	1556	13	1.90E-01	1.77E+01	1.37E+00	3.94E+00	2.15E+01	6.77E+00	8.67E+01	1.70E+02	3.09E+02	5.26E+02	8.14E+02	1.49E+03	1.93E+03
Zircon_091	551	71	0.13	0.0956	0.0011	3.583	0.045	0.2712	0.0026	0.09340	0.00520	0.59	1547	13	1546.9	9.6	1543	21	2.36E-02	1.52E+00	8.84E-01	2.67E+00	2.68E+01	1.28E+00	1.62E+02	4.18E+02	8.38E+02	1.55E+03	2.43E+03	4.52E+03	5.72E+03
Zircon_092	290	98	0.34	0.0792	0.0006	2.218	0.039	0.2029	0.0025	0.06170	0.00160	0.70	1191	13	1186	12	1177	16	5.44E-01	2.15E+01	1.70E+00	5.73E+00	2.96E+01	6.16E+00	1.27E+02	2.34E+02	4.10E+02	7.10E+02	1.08E+03	2.02E+03	2.57E+03
Zircon_093	745	199	0.27	0.0919	0.0025	3.150	0.130	0.2489	0.0046	0.07300	0.00140	0.83	1433	24	1443	31	1464	51	3.76E-01	1.18E+01	1.52E+00	3.61E+00	2.09E+01	1.01E+01	1.26E+02	2.54E+02	5.00E+02	8.81E+02	1.42E+03	2.77E+03	3.69E+03
Zircon_094	616	640	1.04	0.1024	0.0004	4.051	0.042	0.2885	0.0028	0.08390	0.00250	0.78	1634	14	1644.3	8.3	1667.3	6.7	7.51E+00	1.16E+02	1.77E+01	3.06E+01	1.09E+02	5.81E+01	3.77E+02	6.68E+02	1.20E+03	2.05E+03	3.08E+03	5.98E+03	7.98E+03
Zircon_095	707	118	0.17	0.0787	0.0004	2.134	0.025	0.1973	0.0020	0.06180	0.00220	0.73	1161	11	1159.7	8.1	1163.3	9.3	-6.21E-05	9.89E+00	4.42E-01	7.88E-01	3.85E+00	4.83E+00	1.85E+01	3.82E+01	8.50E+01	1.70E+02	3.25E+02	9.53E+02	1.59E+03
Zircon_096	289	139	0.48	0.0883	0.0009	2.935	0.052	0.2400	0.0025	0.06930	0.00210	0.46	1387	13	1391	13	1389	19	3.92E-01	1.76E+01	4.09E+00	1.54E+01	8.63E+01	2.63E+01	3.81E+02	7.03E+02	1.24E+03	2.14E+03	3.15E+03	5.29E+03	6.62E+03
Zircon_097	524	233	0.44	0.0951	0.0020	2.845	0.053	0.2170	0.0024	0.06371	0.00076	0.73	1266	13	1367	14	1529	39	2.83E+00	3.94E+01	7.87E+00	1.37E+01	4.39E+01	2.82E+01	1.63E+02	2.76E+02	5.18E+02	8.53E+02	1.35E+03	2.64E+03	3.44E+03
Zircon_098	227	54	0.24	0.0788	0.0008	2.161	0.064	0.2007	0.0037	0.06320	0.00320	0.40	1179	20	1168	20	1166	19	1.39E-01	1.49E+01	1.23E+00	4.25E+00	1.68E+01	4.80E+00	9.10E+01	1.80E+02	3.38E+02	5.99E+02	8.69E+02	1.78E+03	2.31E+03
Zircon_099	175	36	0.21	0.0853	0.0014	2.637	0.077	0.2256	0.0040	0.06880	0.00370	0.85	1311	21	1314	21	1319	32	1.90E-01	6.36E+00	5.06E-01	2.54E+00	1.22E+01	3.52E+00	6.48E+01	1.24E+02	2.33E+02	4.21E+02	6.49E+02	1.25E+03	1.69E+03
Zircon_100	992	722	0.73	0.0882	0.0033	2.840	0.110	0.2335	0.0036	0.06910	0.00130	0.39	1353	19	1366	28	1387	72	1.52E-01	1.70E+02	3.57E+00	1.20E+01	7.50E+01	5.88E+01	2.43E+02	4.38E+02	8.20E+02	1.39E+03	2.29E+03	5.18E+03	7.07E+03

Note: $^{207}Pb/^{206}Pb$ ratios, ages, and errors are calculated according to Petrus & Kamber (2012).
Analyzed spots were 23 micrometers, using an analytical protocol modified from Solari et al.
Data measured employing a Thermo Xseries QICPMS coupled to a Resonetics, Resolution M050 excimer laser workstation.
[1]U and Th concentrations are calculated employing an external standard zircon as in Paton et al. (2010).
[2]2 sigma uncertainties propagated according to Paton et al., 2010.

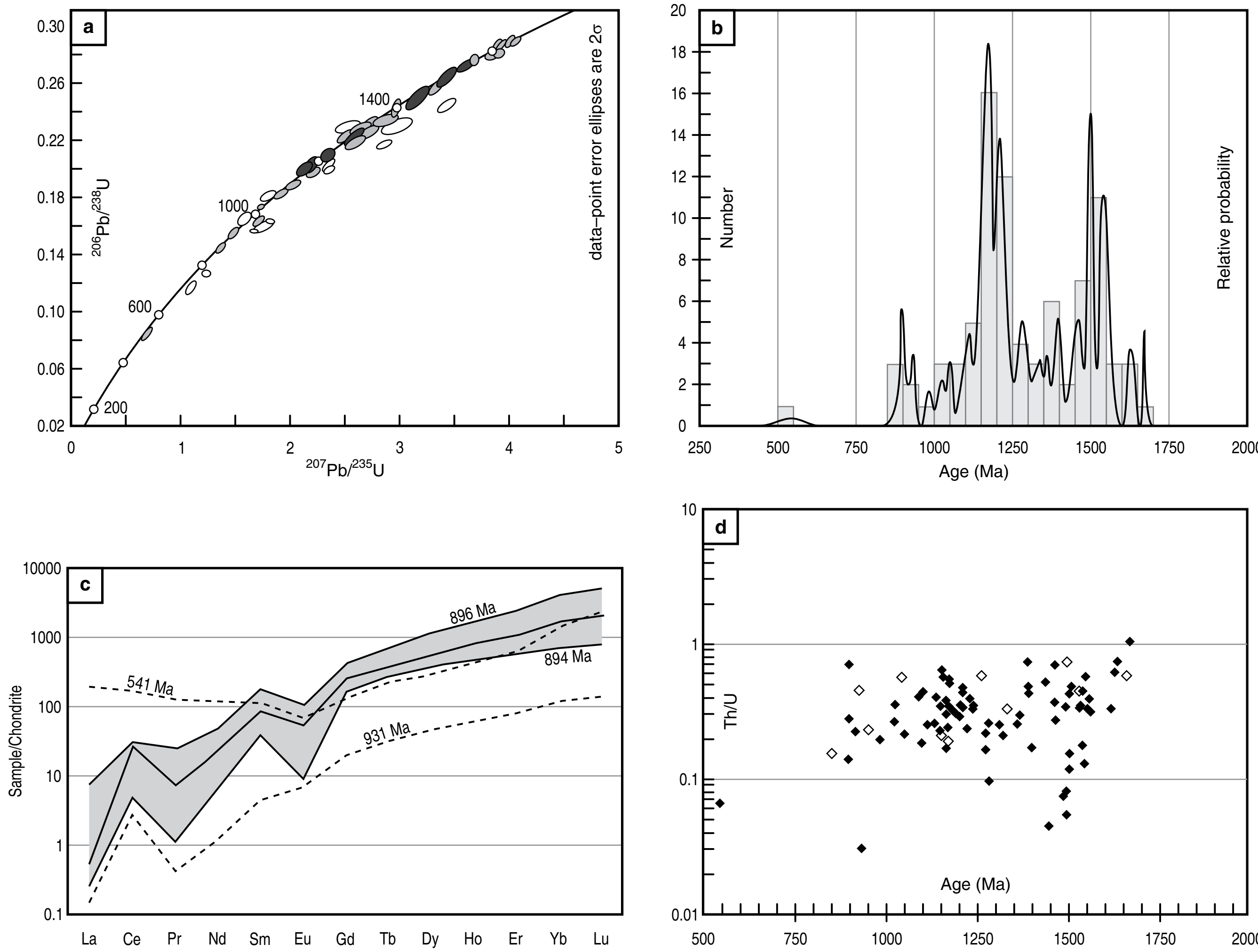

Figure 8. (a) Wetherill concordia diagram of dated zircon spots; dark, filled ellipses correspond to analyses selected for the probability density diagram. **(b)** Probability density plot. **(c)** Chondrite–normalized REE patterns of youngest zircon grains, used to constrain the protolith age. **(d)** Th/U versus age (Ma) diagram; filled symbols correspond to analyses selected for the probability density diagram.

terpret this analysis as reflecting an isotopic mixture between an inherited core and the Paleozoic metamorphism of the sample. A more robust constraint on the depositional age is the youngest population of zircon, which includes three grains that yielded near–identical ages with a mean of 894 ± 8 Ma (MSWD = 0.01). It is therefore likely that the sedimentary protolith of the quartzites and the basic protolith of the interbedded amphibolites of the Anacona Terrane may be Neoproterozoic in age.

5. Comparison with Adjacent Terranes

The main characteristics that allow differentiating the Anacona Terrane from the neighboring Ebéjico and Tahamí Terranes are presented in Table 3. In terms of the basement, the Anacona Terrane is characterized by pre–Carboniferous metamorphic rocks (e.g., the Caldas Amphibolite and its associated metasedimentites); no rocks as old as these are present in the predominantly Permian – Triassic basement of the Tahamí Terrane, while the volcano–sedimentary Ebéjico Terrane lacks medium– or high–grade metamorphic basement. The Ordovician granites present in the Anacona Terrane (e.g., La Miel Orthogneiss) are also absent in the Tahamí and Ebéjico Terranes (Restrepo et al., 2009).

Triassic metamorphic rocks are widespread in the Tahamí Terrane (e.g., Las Palmas Gneiss) but are unknown or not present in either the Cretaceous–aged Ebéjico Terrane or Anacona Terrane. The Tahamí Terrane has well–documented Cretaceous sedimentary cover units (e.g., the Abejorral, San Luis, and San Pablo Formations), and the Ebéjico Terrane is composed of Cretaceous volcano–sedimentary successions. In contrast, no such sedimentary sequences are present in the Anacona Terrane. Finally, the presence of spilites and other low–grade mafic rocks is only reported in the Ebéjico Terrane (Table 3).

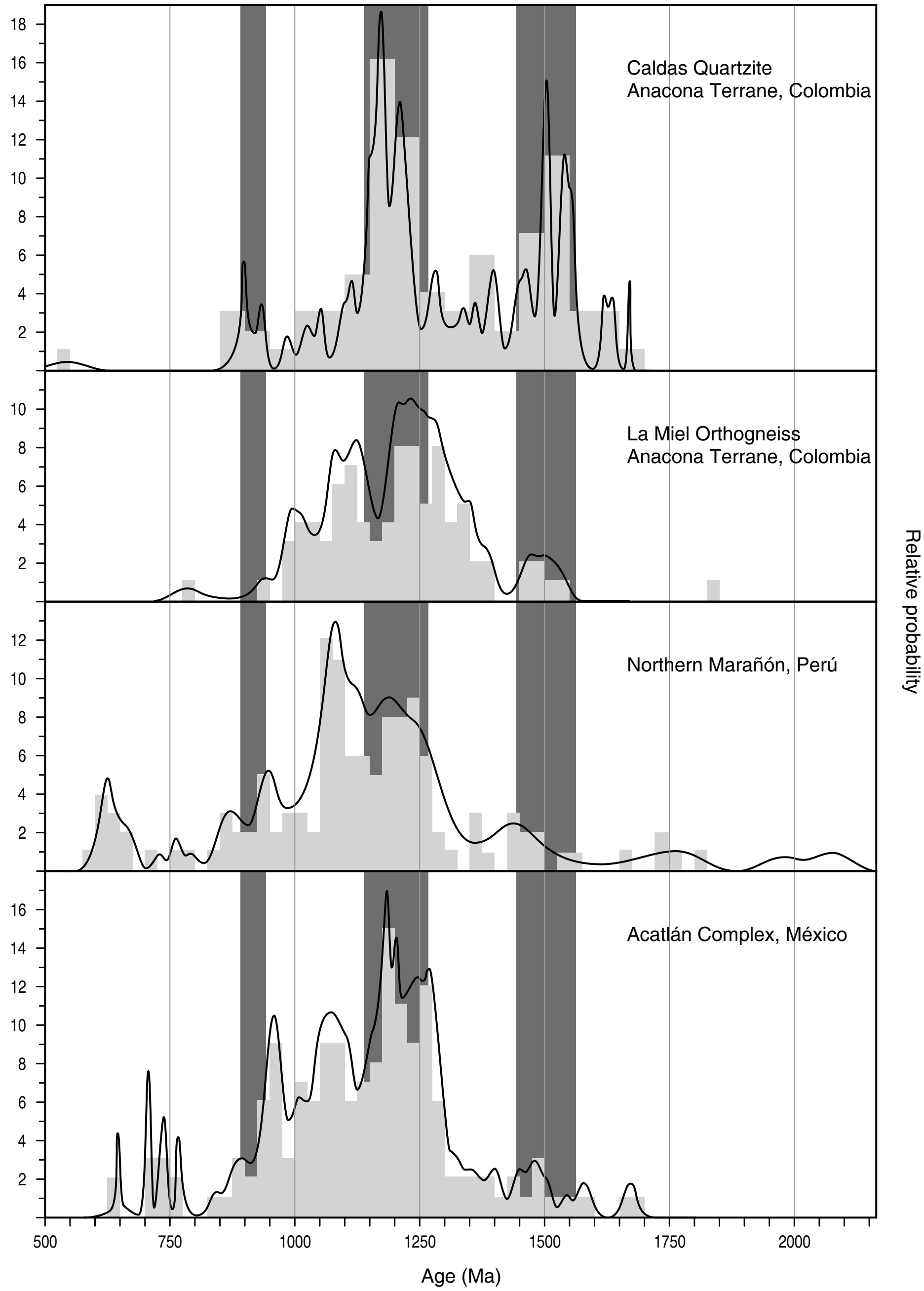

Figure 9. Comparison of probability density plots of quartzite AC–1 and the xenocrystic component in granites of the Acatlán Complex in México, the Marañón Complex in Perú, and the Anacona Terrane in Colombia (modified from Martens et al., 2014 and references therein).

6. Correlatives of the Anacona Terrane in Perú and México

Previous work has correlated the Anacona Terrane with peri–Gondwanan terranes containing relics of an Ordovician magmatic belt that fringed Gondwana (Martens et al., 2014). This Famatinian Orogen is present in South America from Argentina to Venezuela (Ramos, 2018). Potential correlatives are the Mixteca Terrane and the Acatlán Complex in southern México, which initially made part of Gondwana, the early Paleozoic component of the western Marañón Complex in Perú, and the Famatinian magmatic rocks found on the islands off the coast of Perú (Romero et al., 2013). This correlation is supported by the similarity in the ages of xenocrystic zircons from these Ordovician granites in each of these terranes (Figure 9). In the case of the Mexican terranes, the Gondwanan origin has been shown paleontologically (Robison & Pantoja–Alor, 1968; Sánchez–Zavala et al., 1999; Stewart et al., 1999).

Given that no basement rocks similar to those in the Anacona Terrane are known from Ecuador and that the general

Table 3. Comparison between the main characteristics of the Anacona, Ebéjico, and Tahamí Terranes.

Units	Ebéjico	Anacona	Tahamí
Pre–Carboniferous metamorphic rocks	Absent	Present	Absent
Ordovician granites	Absent	Present	Absent
Triassic metamorphic rocks	Absent	Absent	Present
Cretaceous sedimentary rocks	Present	Absent	Present
Spilites and other mafic rocks	Present	Absent	Absent

trend of tectonic transport by the collision of the Caribbean with the South American margin was northward, it is likely that the Anacona Terrane formed further south (in present–day Perú) during the Ordovician, being transported by the north–moving transcurrent faults related to the Cauca–Romeral Fault System. Amalgamation with the Tahamí Terrane occurred at some time between the Jurassic and the end of the Cretaceous (Martens et al., 2014). Given its allochthonous or parautochthonous nature in relation to the Central and Eastern Colombian Andes, all the blocks west of the Anacona Terrane are also necessarily allochthonous or parautochthonous.

7. History of Accretion

The Anacona Terrane does not record a Triassic thermal perturbation of the $^{40}Ar–^{39}Ar$ hornblende or biotite systems. This result indicates that during the main stage of Triassic orogenesis that substantially reworked the Tahamí Terrane, the Anacona Terrane was not nearby. This constraint provides an upper temporal limit on the juxtaposition of the two terranes. Based on the geochronological and field data, we conclude that the Ordovician intrusion of La Miel granite occurred when the amphibolite and biotite schists had already undergone a phase of regional metamorphism as shown by xenoliths of foliated amphibolite within the gneiss. A second phase of metamorphism resulted in the formation of a gneissic foliation in La Miel unit. The timing of this second metamorphic phase has not yet been constrained by U–Pb geochronology, but a $^{40}Ar–^{39}Ar$ hornblende age yields a maximum age constraint of 360 Ma (Restrepo et al., 2008), along with an $^{40}Ar–^{39}Ar$ white mica age of ca. 345 Ma (Vinasco et al., 2006); these mineral ages are currently the best constraints for the onset of cooling following this second metamorphic event. These ages imply that the Anacona Block was not adjacent to the Tahamí Terrane during regional Permian – Triassic metamorphism, and so the terrane docking is post–Triassic.

The Ebéjico Terrane is formed by mafic volcanic rocks interbedded with sedimentary rocks (González, 2001; Jaramillo et al., 2017). The accretion of this block to the Anacona and Tahamí Terranes is thought to have occurred during the Late Cretaceous – Paleogene, dated at 73–65 Ma by Jaramillo et al. (2017) and 70–58 Ma by Zapata & Cardona (2017).

8. Conclusion

The recognition of the Anacona Terrane is significant, despite its relatively small size. It lies along the eastern Cauca–Romeral Fault Zone, a major tectonic boundary in the Colombian Andes that separates a domain of predominantly oceanic affinity in the west from a continental–dominated domain in the east. The terrane is unlike others in the Western or Central Cordilleras, comprising basement rocks with a geologic history spanning the Neoproterozoic – Ordovician. Its medium–pressure metamorphism, xenocrystic and detrital zircon age spectra, and early Paleozoic metamorphism contrast with the low–pressure, Triassic metamorphic basement of the adjacent and much larger Tahamí Terrane. The closest correlative Gondwanan terranes of the Anacona Terrane are in México and Perú. The initial accretion of the Anacona and the Tahamí Terranes occurred in the latest Triassic or later, and we surmise that from a southerly position, the Anacona Terrane was pushed northwards along the Cauca–Romeral Fault by the oblique convergence of the Caribbean Plate located to the northwest.

Acknowledgments

We are grateful to David M. CHEW and Victor A. RAMOS, who improved the manuscript considerably with their suggestions and corrections as reviewers.

References

Andersen, T. 2002. Correction of common lead in U–Pb analyses that do not report ^{204}Pb. Chemical Geology, 192(1–2): 59–79. https://doi.org/10.1016/S0009-2541(02)00195-X

Botero, G. 1963. Contribución al conocimiento de la geología de la zona central de Antioquia. Universidad Nacional de Colombia, Anales de la Facultad de Minas, 57, 101 p. Medellín.

Boynton, W.V. 1984. Cosmochemistry of the rare earth elements: Meteorite studies. Developments in Geochemistry, 2: 63–114. https://doi.org/10.1016/B978-0-444-42148-7.50008-3

Bustamante, A. 2003. Definição das trajetórias P–T–t em rochas metamórficas do flanco ocidental da Cordilheira Central da Colômbia, nas regiões de Caldas e El Retiro. Master thesis, Universidade de São Paulo, 107 p. São Paulo. https://doi.org/10.11606/D.44.2003.tde-26012011-135543

Coney, P.J., Jones, D.L. & Monger, J.W.H. 1980. Cordilleran suspect terranes. Nature, 288(5789): 329–333. https://doi.org/10.1038/288329a0

Correa–Martínez, A.M., Martens, U., Restrepo, J.J., Ordóñez–Carmona, O. & Martins–Pimentel, M. 2005. Subdivisión de las metamorfitas básicas de los alrededores de Medellín–cordillera Central de Colombia. Revista de la Academia Colombiana de Ciencias Exactas, Físicas y Naturales, 29(112): 325–344.

De Paolo, D.J. 1981. Trace element and isotopic effects of combined wallrock assimilation and fractional cristallization. Earth and Planetary Science Letters, 53(2): 189–202. https://doi.org/10.1016/0012-821X(81)90153-9

Echeverría, L.M. 1973. Zonación de las rocas metamórficas del valle de Aburrá y sus alrededores. Bachelor thesis, Universidad Nacional de Colombia, 124 p. Medellín.

Giraldo, M.I. 2010. Esquema geodinámico de la parte noroccidental de la cordillera Central de Colombia. Master thesis, Universidad Nacional de Colombia, 146 p. Medellín.

Giraldo–Ramírez, W. 2013. Caracterización estructural y geoquímica del bloque Anacona. Bachelor thesis, Universidad Nacional de Colombia, 91 p. Medellín.

González, H. 1980. Geología de las planchas 167 Sonsón y 187 Salamina. Scale 1:100 000. Ingeominas, Internal report 1760, 262 p. Medellín.

González, H. 2001. Memoria explicativa: Mapa geológico del departamento de Antioquia. Scale 1:400 000. Ingeominas, 240 p. Medellín.

Grosse, E. 1926. Estudio geológico del terciario carbonífero de Antioquia en la parte occidental de la cordillera Central de Colombia, entre el río Arma y Sacaojal, ejecutado en los años de 1920–1923. Dietrich Reimer, 361 p. Berlin.

Hoffman, P.F. 1989. Precambrian geology and tectonic history of North America. In: Bally, A.W. & Palmer, A.R. (editors), The geology of North America–An overview. Geological Society of America, A: 447–511. Boulder, USA. https://doi.org/10.1130/DNAG-GNA-A.447

Hofmann, A.W. 1988. Chemical differentiation of the Earth: The relationship between mantle, continental crust, and oceanic crust. Earth and Planetary Science Letters, 90(3): 297–314. https://doi.org/10.1016/0012-821X(88)90132-X

Ibañez–Mejia, M., Ruiz, J., Valencia, V.A., Cardona, A., Gehrels, G.E. & Mora, A. 2011. The Putumayo Orogen of Amazonia and its implications for Rodinia reconstructions: New U–Pb geochronological insights into the Proterozoic tectonic evolution of northwestern South America. Precambrian Research, 191(1–2): 58–77. https://doi.org/10.1016/j.precamres.2011.09.005

Jaramillo, J.S., Cardona, A., León, S., Valencia, V. & Vinasco, C. 2017. Geochemistry and geochronology from Cretaceous magmatic and sedimentary rocks at 6° 35' N, western flank of the Central Cordillera (Colombian Andes): Magmatic record of arc growth and collision. Journal of South American Earth Sciences, 76: 460–481. https://doi.org/10.1016/j.jsames.2017.04.012

Jones, D.L., Howell, D.G., Coney, P.J. & Monger, J.W.H. 1983. Recognition, character and analysis of tectonostratigraphic terranes in western North America. Journal of Geological Education, 31(4): 295–303.

Martens, U., Weber, B. & Valencia, V. 2010. U/Pb geochronology of Devonian and older Paleozoic beds in the southeastern Maya Block, Central America: Its affinity with peri–Gondwanan terranes. Geological Society of America Bulletin, 122(5–6): 815–829. https://doi.org/10.1130/B26405.1

Martens, U., Restrepo, J.J., Ordóñez–Carmona, O. & Correa–Martínez, A.M. 2014. The Tahamí and Anacona Terranes of the Colombian Andes: Missing links between South American and Mexican Gondwana margins. The Journal of Geology, 122(5): 507–530. https://doi.org/10.1086/677177

Maya, M. & Escobar, A. 1985. Estudio de las rocas metamórficas entre el Ancón sur y la quebrada La Miel, Caldas, Antioquia. Bachelor thesis, Universidad Nacional de Colombia, 160 p. Medellín.

Maya, M. & González, H. 1995. Unidades litodémicas en la cordillera Central de Colombia. Boletín Geológico, 35(2–3): 43–57.

Michard, A., Gurriet, P., Soudant, M. & Albarede, F. 1985. Nd isotopes in French Phanerozoic shales: External vs. internal aspects of crustal evolution. Geochimica et Cosmochimica Acta, 49(2): 601–610. https://doi.org/10.1016/0016-7037(85)90051-1

Ortega–Gutiérrez, F., Ruiz, J. & Centeno–García, E. 1995. Oaxaquia: A Proterozoic microcontinent accreted to North America during the late Paleozoic. Geology, 23(12): 1127–1130. https://doi.org/10.1130/0091-7613(1995)023<1127:OAPMAT>2.3.CO;2

Patiño, J.J. & Noreña, J.A. 1984. Estudio de las rocas metamórficas en la parte sur del municipio de Caldas, Antioquia. Bachelor thesis, Universidad Nacional de Colombia, 154 p. Medellín.

Paton, C., Woodhead, J.D., Hellstrom, J.C., Hergt, J.M., Greig, A. & Maas, R. 2010. Improved laser ablation U–Pb zircon geochronology through robust downhole fractionation correction. Geochemistry, Geophysics, Geosystems, 11(3): 1–36. https://doi.org/10.1029/2009GC002618

Petrus, J.A. & Kamber, B.S. 2012. VizualAge: A novel approach to laser ablation ICP–MS U–Pb geochronology data reduction. Geostandards and Geoanalytical Research, 36(3): 247–270. https://doi.org/10.1111/j.1751-908X.2012.00158.x

Ramos, V.A. 2018. The Famatinian orogen along the protomargin of western Gondwana: Evidence for a nearly continuous Ordovician magmatic arc between Venezuela and Argentina. In: Folguera, A., Contreras–Reyes, E., Heredia, N., Encinas, A., Iannelli, S.B., Oliveros, V., Dávila, F.M., Collo, G., Giambiagi, L., Maksymowicz, A., Iglesia–Llanos, M.P., Turienzo, M., Naipauer, M., Orts, D., Litvak, V., Alvarez, O., Arriagada, C. (editors), The evolution of the Chile–Argentinean Andes. Springer Earth System Sciences. Springer, p. 133–161. https://doi.org/10.1007/978-3-319-67774-3_6

Restrepo, J.J. 1986. Metamorfismo en el sector norte de la cordillera Central de Colombia. Universidad Nacional de Colombia, Trabajo presentado como requisito parcial para la promoción a Profesor Titular. Unpublished report, 195 p. Medellín.

Restrepo, J.J. 2008. Obducción y metamorfismo de ofiolitas triásicas en el flanco occidental del Terreno Tahamí, cordillera Central de Colombia. Boletín Ciencias de la Tierra, (22): 49–100.

Restrepo, J.J. & Toussaint, J.F. 1977. Anfibolitas granatíferas de Caldas, Antioquia. Boletín Ciencias de la Tierra, (2): 147–154.

Restrepo, J.J. & Toussaint, J.F. 1978. Ocurrencia de Precámbrico en las cercanías de Medellín, cordillera Central de Colombia. Publicaciones Especiales de Geología, 12: 1–11.

Restrepo, J.J. & Toussaint, J.F. 1984. Unidades litológicas de los alrededores de Medellín. Primera conferencia sobre riesgos geológicos del valle de Aburrá. Sociedad Colombiana de Geología. Memoirs, p. 1–26. Medellín.

Restrepo, J.J. & Toussaint, J.F. 2020. Tectonostratigraphic terranes in Colombia: An update. First part: Continental terranes. In: Gómez, J. & Mateus–Zabala, D. (editors), The Geology of Colombia, Volume 1 Proterozoic – Paleozoic. Servicio Geológico Colombiano, Publicaciones Geológicas Especiales 35, p. 37–63. Bogotá. https://doi.org/10.32685/pub.esp.35.2019.03

Restrepo, J.J., Toussaint, J.F., González, H., Cordani, U., Kawashita, K., Linares, E. & Parica, C. 1991. Precisiones geocronológicas sobre el occidente colombiano. Simposio sobre magmatismo andino y su marco tectónico, Programa Internacional de Ciencias Geológicas. Memoirs, I, p. 1–21. Manizales.

Restrepo, J.J., Dunlap, W.J., Martens, U., Ordóñez–Carmona, O. & Correa–Martínez, A.M. 2008. Ar–Ar ages of amphibolites from the Central Cordillera of Colombia and their implications for tectonostratigraphic terrane evolution in the northwestern Andes. VI South American Symposium on Isotope Geology. Proceedings CD ROM, p. 1–6. Bariloche, Argentina.

Restrepo, J.J., Ordóñez–Carmona, O., Martens, U. & Correa–Martínez, A.M. 2009. Terrenos, complejos y provincias en la cordillera Central de Colombia. Ingeniería, Investigación y Desarrollo, 9(2): 49–56.

Robison, R.A. & Pantoja–Alor, J. 1968. Tremadocian trilobites from the Nochixtlán region, Oaxaca, Mexico. Journal of Paleontology, 42(3): 767–800.

Romero, D., Valencia, K., Alarcón, P., Peña, D. & Ramos, V.A. 2013. The offshore basement of Perú: Evidence for different igneous and metamorphic domains in the forearc. Journal of South American Earth Sciences, 42: 47–60. https://doi.org/10.1016/j.jsames.2012.11.003

Sánchez–Zavala, J.L., Centeno–García, E. & Ortega–Gutiérrez, F. 1999. Review of Paleozoic stratigraphy of México and its role in the Gondwana–Laurentia connections. In: Ramos, V.A. & Keppie, J.D. (editors), Laurentia–Gondwana connections before Pangea. Geological Society of America, Special Paper 336, p. 211–226. https://doi.org/10.1130/0-8137-2336-1.211

Sepúlveda, R.D. & Saldarriaga, S.M. 1980. Metamorfismo de las rocas del oriente del municipio de Caldas, Antioquia. Bachelor thesis, Universidad Nacional de Colombia, 115 p. Medellín.

Siivola, J. & Schmid, R. 2007. List of mineral abbreviations. In: Fettes, D. & Desmons, J. (editors), Metamorphic rocks: A classification and glossary terms. Cambridge University Press, p. 93–110.

Solari, L., Gómez–Tuena, A., Bernal, J.P., Pérez–Arvizu, O. & Tanner, M. 2010. U–Pb zircon geochronology with an integrated LA–ICP–MS microanalytical workstation: Achievements in precision and accuracy. Geostandards and Geoanalytical Research, 34(1): 5–18. https://doi.org/10.1111/j.1751-908X.2009.00027.x

Stewart, J.H., Blodgett, R.B., Boucot, A.J., Carter, J.L. & López, R. 1999. Exotic Paleozoic strata of Gondwanan provenance near Ciudad Victoria, Tamaulipas, México. In: Ramos, V.A. & Keppie, J.D. (editors), Laurentia–Gondwana connections before Pangea. Geological Society of America, Special Paper 336, p. 227–252. https://doi.org/10.1130/0-8137-2336-1.227

Sun, S.S. & McDonough, W.F. 1989. Chemical and isotopic systematics of oceanic basalts: Implications for mantle composition and processes. In: Saunders, A.D. & Norry, M.J. (editors), Magmatism in the ocean basins. Geological Society of London, Special Publication 42, p. 313–345. https://doi.org/10.1144/GSL.SP.1989.042.01.19

Tassinari, C.C.G., Bettencourt, J.S., Geraldes, M.C., Macambira, M.J.B. & Lafon, J.M. 2000. The Amazonian Craton. In: Cordani, U.G., Milani, E.J., Thomaz–Filho, A. & Campos, D.A. (editors), Tectonic evolution of South America. 31st International Geological Congress. Proceedings, p. 41–95. Rio de Janeiro, Brazil.

Toussaint, J.F. & Restrepo, J.J. 1989. Acreciones sucesivas en Colombia: Un nuevo modelo de evolución geológica. V Congreso Colombiano de Geología. Memoirs, I, p. 127–146. Bucaramanga.

Villagómez, D., Spikings, R., Magna, T., Kammer, A., Winkler, W. & Beltrán, A. 2011. Geochronology, geochemistry and tectonic evolution of the Western and Central Cordilleras of Colombia. Lithos, 125(3–4): 875–896. https://doi.org/10.1016/j.lithos.2011.05.003

Vinasco, C.J., Cordani, U.G., González, H., Weber, M. & Peláez, C. 2006. Geochronological, isotopic, and geochemical data from Permo–Triassic granitic gneisses and granitoids of the Colombian central Andes. Journal of South American Earth Sciences, 21(4): 355–371. https://doi.org/10.1016/j.jsames.2006.07.007

Wasteneys, H.A., Clark, A.H., Farrar, E. & Langridge, R.J. 1995. Grenvillian granulite–facies metamorphism in the Arequipa Massif, Peru: A Laurentia–Gondwana link. Earth and Planetary Science Letters, 132(1–4): 63–73. https://doi.org/10.1016/0012-821X(95)00055-H

Zapata, J.P. & Cardona, A. 2017. Unidades miloníticas asociadas a eventos colisionales del Cretácico Superior en el margen occidental de la cordillera Central. XVI Congreso Colombiano de Geología and III Simposio de Exploradores. Memoirs, p. 1889–1891. Santa Marta.

Explanation of Acronyms, Abbreviations, and Symbols:

CL	Cathodoluminescence
E–MORB	Enriched mid–ocean ridge basalt
LA–ICP–MS	Laser ablation inductively coupled plasma mass spectrometry
Low–P	Low pressure
MORB	Mid–ocean ridge basalt
MSWD	Mean square weighted deviation
N–MORB	Normal mid–ocean ridge basalt
OIB	Ocean island basalt
PT	Pressure and temperature
REE	Rare earth element
UNAM	Universidad Nacional Autónoma de México

Authors' Biographical Notes

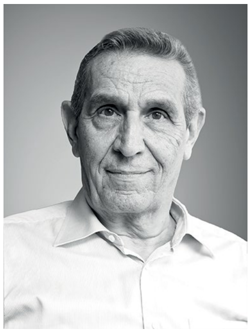

Jorge Julián RESTREPO obtained a degree in mining engineering and metallurgy at the Universidad Nacional de Colombia in 1968 and a Master of Science degree in geology at the Colorado School of Mines in 1973. He was a faculty member of the Universidad Nacional de Colombia Sede Medellín, for over 40 years and currently holds the titles of Emeritus Professor and "Maestro Universitario". He taught Mineralogy, Metamorphic Petrology, Regional Geology, Field Geology, and Geochronology. His research focused on plate tectonics applied to the geology of Colombia, tectonostratigraphic terranes, geochronology, and the geologic evolution of metamorphic and mafic/ultramafic complexes of the Central Cordillera. Other interests are photography, genealogy, and the study of passifloras.

Uwe MARTENS graduated with a degree in geological engineering from the Universidad Nacional de Colombia, Sede Medellín, and a PhD in geological and environmental science from Stanford University. He has taught at the Universidad Nacional de Colombia, San Carlos National University in Guatemala, and Stanford University. He currently is a visiting researcher at Centro de Geociencias, UNAM, México and works as an independent consultant in the field of source–to–sink analysis.

Wilmer E. GIRALDO–RAMÍREZ is a geological engineer who graduated from the Universidad Nacional de Colombia Sede Medellín (2014) and has a Master of Science degree in basins and mobile belt analysis from the Universidade do Estado do Rio de Janeiro (2017). He has worked at institutions such as the Universidad Nacional de Colombia, Universidad Católica de Oriente, Corporación Autónoma Regional de las Cuencas de los Ríos Negro y Nare "Cornare" and city of Marinilla. His main interests are the geodynamic evolution of the northern Andes, and he has secondary interests in the land use planning of eastern Antioquia, biology of *Passiflora* and sports including rugby and Brazilian jiu–jitsu.

Carboniferous

Devonian